

Nuclear matter from the ladder resummation in terms of the experimental nucleon-nucleon scattering amplitudes

J. M. Alarcón*

*Universidad de Alcalá, Grupo de Física Nuclear y de Partículas, Departamento de Física y Matemáticas,
28805 Alcalá de Henares (Madrid), Spain*

J. A. Oller[†]

Departamento de Física, Universidad de Murcia, 30071 Murcia, Spain



(Received 19 December 2022; revised 15 March 2023; accepted 31 March 2023; published 26 April 2023)

Infinite nuclear matter is studied by resumming the series of ladder diagrams based on the results developed by us [*Ann. Phys. (NY)* **437**, 168741 (2022)]. The master formula for the energy density is explicitly solved for the case of contact interactions, within a pionless description of the nucleon-nucleon interactions. Renormalized results are obtained which are directly expressed in terms of the nucleon-nucleon phase shifts and mixing angles in partial-wave amplitudes up to and including G waves, with convergence reached under the inclusion of higher partial waves. The energy per particle, density, and sound velocity resulting from the ladder series are given for symmetric and neutron matter. This resummation of the ladder diagrams provides a rigorous result that may be used as low-density reference for other parametrizations of $\bar{\mathcal{E}}$ for higher densities.

DOI: [10.1103/PhysRevC.107.044319](https://doi.org/10.1103/PhysRevC.107.044319)

I. INTRODUCTION

The rise of precision physics has brought a need for more rigorous calculations in the low energy sector of QCD. In order to interpret such experiments' outcome correctly and claim a possible discovery, theoretical calculations with controlled systematic errors are crucial. The properties of baryonic matter have been studied for such kind of programs. In that case, there is additional complication besides dealing with low energy QCD, since the interactions occur in a baryonic environment, and vacuum approaches are not applicable.

In this paper we apply many-body field theory to the calculation of the energy per particle $\bar{\mathcal{E}}$ for nuclear matter, and other magnitudes that can be deduced thereof. We define nuclear matter as an infinite uniform system of nucleons interacting by the strong force without electromagnetic interactions. This system is supposed to approximate the interior of a heavy nucleus. The proportion of protons and neutrons in the system is controlled by the fraction of protons x_p , so that for $x_p = 0$ one has pure neutron matter (PNM) and $x_p = 1/2$ corresponds to symmetric nuclear matter (SNM), both being extremes of special interest in our research here. Indeed, the equation of state of nuclear matter is nowadays one of the most active fields where these types of calculations are necessary, especially in the study of neutron stars and gravitational waves. The former offers a unique possibility of studying nuclear matter under extreme conditions and testing our current theoretical approaches for baryonic matter.

The many-body calculations within perturbation theory [1] have long been well known [2–8]. However, for larger scattering lengths the perturbative expansion in powers of $a_0 k_F$ fails, with a_0 the S -wave scattering length. Of course, this is the case if one is interested in the unitary limit $|a_0 k_F| \rightarrow \infty$ [9–11], which is closely related to neutron matter due to the large and negative neutron-neutron (nn) scattering length $a_{nn} = -18.95 \pm 0.40$ fm [12]. Note that $|a_{nn}| \gg m_\pi^{-1}$, with m_π the pion mass and whose inverse typically controls the longest range of strong interactions.

A time-honored possibility to end with a meaningful result for large scattering lengths is to resum the two-body interactions in the medium [1]. In the Brueckner theory [13–17] the infinite series of interacting particle-particle intermediate states is resummed, where the two particles always have momenta above their Fermi momenta.¹ This theory was generalized by Thouless [18] considering also two-fermion intermediate states with momenta below the Fermi momenta (or intermediate hole-hole states). The notation of ladder diagrams was also introduced by him to denote the associated Feynman graphs. As a result, both particle-particle and hole-hole intermediate states interact between two consecutive rungs of the ladder series, and their infinite iteration is resummed. The ladder resummation at zero temperature is studied Refs. [19–22], taking into account Pauli blocking without including self-energy effects. Resumming the ladder diagrams in such circumstances is typically considered a good starting point for calculating $\bar{\mathcal{E}}$ [19,23,24], also supported by the power counting arguments of Ref. [20,25,26].

*jmanuel.alarcon@uah.es

†oller@um.es

¹The Fermi momenta are globally denoted by k_F or ξ .

When the interaction between two spin-1/2 fermions is reduced to its scattering length, an algebraic renormalized formula for the ladder resummation was accomplished by Kaiser in Ref. [21]. Within only dimensional regularization, the extension of the previous result for taking also into account the contributions from the effective range in S wave was obtained by the same author in Ref. [22] where, due to off-shell effects, the resulting formula was conjectured and checked up to some order. The case of an interaction given by the P -wave scattering volume a_1 was separately discussed in the same reference, and the resummation within dimensional regularization was accomplished. The connection between the ladder resummation and the density-functional theory in many-body calculations was studied in [27,28]. Furthermore, it is conjectured [29,30] that, for nuclear and atomic systems with two-body interactions near the unitary limit, the binding energy of the three-body system defines the relevant scale for low-energy observables, such as particle energy.

We recently resummed the ladder diagrams for arbitrary spin-1/2 fermion-fermion interactions in vacuum in Ref. [31]. The resummation can take into account higher orders in the effective range expansion (ERE) of a partial-wave amplitude (PWA) and/or any number of PWAs. The case of contact interactions is fully resolved and renormalized results for $\bar{\mathcal{E}}$ are obtained, so that they are directly expressed in terms of vacuum scattering parameters of the ERE. In the present work we proceed further, and derive the needed equations for different Fermi momenta ξ_1 (protons) and ξ_2 (neutrons). In addition, we give the expression for $\bar{\mathcal{E}}$ when infinitely many orders are included in the ERE for (un)coupled PWAs, such that the resulting $\bar{\mathcal{E}}$ is directly expressed in terms of phase shifts and mixing angles. In this way, the results from the ladder resummation are completely independent of cutoff and have no free parameters. We have then explored the cases of SNM and PNM, discussing $\bar{\mathcal{E}}$ for both cases, and its first and second order derivatives, namely, the pressure (or the equation of state) and the sound velocity. For the case of PNM our results at low densities have been extrapolated towards larger densities by using a quadratic expression in x_p . Results compatible with present-day constraints and determinations are obtained for the symmetry energy S_0 and its logarithmic slope in density L at nuclear matter saturation.

The contents of the paper are organized as follows. After this Introduction, the resummation of the ladder diagrams and its partial-wave decomposition are discussed in Sec. II. An important needed element is the in-medium nucleon-nucleon scattering amplitude which is discussed in Sec. III, and solved in Sec. IV for the case of contact interactions. The results for SNM and PNM are given in Sec. V. The last section contains a summary and concluding remarks.

II. RESUMMATION OF LADDER DIAGRAMS FOR THE ENERGY DENSITY \mathcal{E}

The resummation of the ladder diagrams for evaluating \mathcal{E} in terms of an arbitrary fermion-fermion vacuum T matrix was accomplished by us in Ref. [31]. This derivation was based on the many-body formalism of Ref. [32], which we refer to as the in-medium many-body quantum field theory. Since the resummation of ladder diagrams was derived in detail in Ref. [31], here we only provide a brief summary signaling the main steps in the derivation. We also briefly recap the power counting of Ref. [25] for in-medium calculations.

A. Summary of the in-medium many-body formalism of Ref. [32]

Reference [32] determines the in-medium Lagrangian after integrating out the fermions in the nuclear medium. This is accomplished by calculating the generating functional $\mathcal{Z}[J]$ of in-medium Green functions with external sources J .

The vacuum Lagrangian contains a pure bosonic part, \mathcal{L}_ϕ , and another bilinear in the fermion fields, that is globally called $\mathcal{L}_{\bar{\psi}\psi} = \bar{\psi}D\psi$. The operator D , which we write as $D = D_0 - A$, comprises the free fermion Lagrangian $D_0 = i\gamma^\mu\partial_\mu - m$, with m the nucleon mass in the isospin limit, and the interacting part A , which incorporates the boson-fermion interactions and external sources. The bosons can be either light, e.g., pions, or heavy ones which, when integrated out, give rise to contact multifermion interactions. In this way, we do not need to additionally incorporate monomials with extra fermion fields in the Lagrangian density, like quartic ones $\mathcal{L}_{\bar{\psi}\bar{\psi}\psi\psi}$ and so on. The result for $e^{i\mathcal{Z}[J]}$ calculated in Ref. [32] can be written as

$$\begin{aligned}
 e^{i\mathcal{Z}[J]} = & \int [dU] \exp \left[i \int dx \mathcal{L}_\phi - i \int \frac{d\mathbf{p}}{(2\pi)^3} \int \text{Tr} (A [I - D_0^{-1}A]^{-1} |_{(x,y)} n(p)) dx dy e^{ip(x-y)} \right. \\
 & - \frac{1}{2} (-i)^2 \int \frac{d\mathbf{p}}{(2\pi)^3} \int \frac{d\mathbf{q}}{(2\pi)^3} \int \text{Tr} (A [I - D_0^{-1}A]^{-1} |_{(x,x')} n(q) A [I - D_0^{-1}A]^{-1} |_{(y',y)} n(p)) \\
 & \left. \times e^{ip(x-y)} e^{-iq(x'-y')} dx dx' dy dy' + \dots \right], \tag{2.1}
 \end{aligned}$$

such that the exponent in the integrand is i times the total in-medium Lagrangian. In this equation each trace is taken over the spin and other internal indices of the fermions, like the isospin ones, and D_0^{-1} is the free vacuum fermion propagator. In isospin matrix notation

$$n(p) = \begin{pmatrix} \theta(\xi_1 - |\mathbf{p}|) & 0 \\ 0 & \theta(\xi_2 - |\mathbf{p}|) \end{pmatrix}, \tag{2.2}$$

where $\theta(x)$ is the Heaviside or step function, and it restricts the momentum \mathbf{p} below the Fermi momentum ξ_α for each nucleon species α , with $\alpha = 1$ (2) referring to a proton (neutron).² Each term in the sum in Eq. (2.1) involving at least one $n(p)$ is denoted as an in-medium generalized vertex (IGV), after Ref. [32], and its total number is called V_ρ . The IGVs are made by sewing nonlocal vacuum vertices Γ ,

$$\Gamma \equiv -iA[I - D_0^{-1}A]^{-1} = -iA \sum_{n=0}^{\infty} (D_0^{-1}A)^n, \quad (2.3)$$

with Fermi seas, with each of them involving a factor $n(p)$. In addition, there is a numerical factor $(-1)^{n+1}/n$ from the series of $\ln(1 + \varepsilon)$.

Equation (2.1) gives rise to Feynman rules and graphs. The associated propagators for the fermion lines are either in-medium insertions of on-shell Fermi seas, connecting Γ vertices, or fermion vacuum propagators joining vacuum vertices A . In the following, a pure vacuum fermion propagator $iD_0^{-1}(p)$ is depicted as a solid line, and a Fermi-sea insertion $n(p)(2\pi)\delta(p^0 - \mathbf{p}^2/2m)$ is drawn by a double line. In both cases one has to sum over spin and isospin indices, and integrate over the intermediate four-momentum $\int d^4p/(2\pi)^4$. Each vertex $-iA$ is plotted as a filled circle, while the non-local Γ vertices are plotted as empty circles. Additionally, one should keep in mind that bosonic and source lines can stem from the A vertices. Of course, we refer to the original Ref. [32] for the derivation and more extensive discussion of this many-body framework. A good illustration is the pure perturbative calculations done in Ref. [26] (see also Refs. [33,34]), and nonperturbative ones were undertaken in Refs. [20,25,35,36]. For a recent review see Ref. [37].

B. Fock and Hartree diagram contributions to \mathcal{E}

Reference [31] performs the resummation of the ladder diagrams to calculate the energy density \mathcal{E} of a system of fermions of spin 1/2 with an arbitrary vacuum fermion-fermion T matrix, which we call t . Here, we first give the formula obtained in Ref. [31], and then introduce the different operators that appear in it.

The resulting expression for the interacting part of \mathcal{E} in the ladder approximation, $\mathcal{E}_{\mathcal{L}}$, is [31]

$$\mathcal{E}_{\mathcal{L}} = i \text{Tr} \left(\sum_{n=1}^{\infty} \frac{(t_m L_d)^n}{2n} \right) = -\frac{i}{2} \text{Tr} \ln (I - t_m L_d), \quad (2.4)$$

$$L_d(p, \mathbf{a}) = i \frac{mp}{16\pi^2} \sum_{\sigma, \alpha} \int d\hat{\mathbf{k}} \theta(\xi_{\alpha_1} - |\mathbf{a} + p\hat{\mathbf{k}}|) \theta(\xi_{\alpha_2} + |\mathbf{a} - p\hat{\mathbf{k}}|) |p\hat{\mathbf{k}}\sigma_1\sigma_2\alpha_1\alpha_2\rangle_{AA} \langle p\hat{\mathbf{k}}\sigma_1\sigma_2\alpha_1\alpha_2|, \quad (2.8)$$

$$L_m(p, \mathbf{a}) = -\frac{m}{2} \sum_{\sigma, \alpha} \int \frac{d^3k}{(2\pi)^3} \frac{\theta(\xi_{\alpha_1} - |\mathbf{a} + \mathbf{k}|) + \theta(\xi_{\alpha_2} - |\mathbf{a} - \mathbf{k}|)}{\mathbf{k}^2 - \mathbf{p}^2 - i\epsilon} |\mathbf{k}\sigma_1\sigma_2\alpha_1\alpha_2\rangle_{AA} \langle \mathbf{k}\sigma_1\sigma_2\alpha_1\alpha_2|. \quad (2.9)$$

²The Fermi momentum could also depend on the nucleon but we do not consider further this case because our interest here rests in unpolarized Fermi systems.

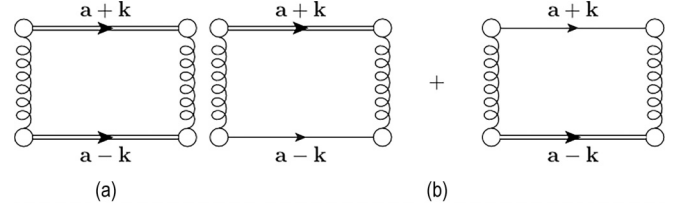


FIG. 1. In panel (a) we show $L_d(p, \mathbf{a})$ and in panel (b) $L_m(p, \mathbf{a})$, which comprises two Feynman diagrams. The double lines correspond to Fermi seas insertions. Here, a spring schematically indicates any expanded interaction with momentum flow $\pm \mathbf{k}$ along it.

with the series fixing the branch of $\ln z$, with $\arg z \in (-\pi, \pi)$. In this equation the in-medium fermion-fermion T matrix is denoted by t_m , while L_d is a unitary loop function made up of two Fermi-sea insertions, which is shown in the panel (a) of Fig. 1.

In addition to the interacting part, one also has to sum the densities of kinetic energies, \mathcal{E}_K , of protons and neutrons:

$$\mathcal{E}_K = \frac{\xi_1^5}{10m\pi^2} + \frac{\xi_2^5}{10m\pi^2} = \rho_1 \frac{3\xi_1^2}{10m} + \rho_2 \frac{3\xi_2^2}{10m}. \quad (2.5)$$

Given the four-momenta k_1 and k_2 of the two fermions, we introduce the four-vectors

$$\begin{aligned} a &= \frac{1}{2}(k_1 + k_2), \\ k &= \frac{1}{2}(k_1 - k_2), \end{aligned} \quad (2.6)$$

so that

$$k_1 = a + k, \quad k_2 = a - k. \quad (2.7)$$

For the on-shell case we use \mathbf{p} instead of \mathbf{k} to denote the relative momentum, with $p \equiv |\mathbf{p}|$, so that $k_i^0 = E(\mathbf{p}_i) = p_i^2/2m$. It is important to keep in mind that the total four-momentum a is conserved during the in-medium scattering process of two fermions because of translational symmetry.

There are two important in-medium unitary functions. One is $L_d(p, \mathbf{a})$, already mentioned, and the other is $L_m(p, \mathbf{a})$, which consists of two mixed intermediate states composed of a Fermi sea insertion and a vacuum propagator. The loop function $L_m(p, \mathbf{a})$ is depicted in panel (b) of Fig. 1. These loop-function operators are given by the expressions

Here, we have denoted by $|p\mathbf{k}\sigma_1\sigma_2\alpha_1\alpha_2\rangle_A$ the antisymmetric two-fermion intermediate state with momenta $\mathbf{k}_1 = \mathbf{a} + \mathbf{k}$, $\mathbf{k}_2 = \mathbf{a} - \mathbf{k}$, third components of spin σ_1 , σ_2 , and third components of isospin α_1 , α_2 . The sum over the spin and isospin indices σ_i and α_i is denoted by $\sum_{\sigma, \alpha}$. A symmetry factor 1/2

is included in Eqs. (2.8) and (2.9) because the two-fermion state is antisymmetric. In these equations we have also taken into account that, as the in-medium states summed over in the trace of Eq. (2.4) are on shell,

$$2ma^0 - \mathbf{a}^2 = m[E(\mathbf{a} + \mathbf{p}) + E(\mathbf{a} - \mathbf{p})] - \mathbf{a}^2 = \mathbf{p}^2. \quad (2.10)$$

In terms of the vacuum T -matrix t and L_m , the operational equation that defines $t_m(\mathbf{a})$ is [31]

$$t_m(\mathbf{a}) = t + tL_m(p, \mathbf{a})t_m(\mathbf{a}). \quad (2.11)$$

In this way, the in-medium T matrix $t_m(\mathbf{a})$ results by iterating t with mixed intermediate states making up L_m . From this equation and Eq. (2.9), the matrix elements of $t_m(\mathbf{a})$ between the initial and final two-fermion antisymmetric states, $|\mathbf{p}\sigma_1\sigma_2\alpha_1\alpha_2\rangle$ and $|\mathbf{p}'\sigma'_1\sigma'_2\alpha'_1\alpha'_2\rangle$, respectively, fulfill the integral equation (IE)

$$\begin{aligned} & \langle \mathbf{p}'\sigma'_1\sigma'_2\alpha'_1\alpha'_2 | t_m(\mathbf{a}) | \mathbf{p}\sigma_1\sigma_2\alpha_1\alpha_2 \rangle \\ &= \langle \mathbf{p}'\sigma'_1\sigma'_2\alpha'_1\alpha'_2 | t(\mathbf{a}) | \mathbf{p}\sigma_1\sigma_2\alpha_1\alpha_2 \rangle \\ & - \frac{m}{2} \sum_{\tilde{\sigma}, \tilde{\alpha}} \int \frac{d^3k}{(2\pi)^3} \langle \mathbf{p}'\sigma'_1\sigma'_2\alpha'_1\alpha'_2 | t(\mathbf{a}) | \mathbf{k}\tilde{\sigma}_1\tilde{\sigma}_2\tilde{\alpha}_1\tilde{\alpha}_2 \rangle \\ & \times \frac{\theta(\xi_1 - |\mathbf{a} + \mathbf{k}|) + \theta(\xi_2 - |\mathbf{a} - \mathbf{k}|)}{\mathbf{k}^2 - \mathbf{p}^2 - i\epsilon} \\ & \times \langle \mathbf{k}\tilde{\sigma}_1\tilde{\sigma}_2\tilde{\alpha}_1\tilde{\alpha}_2 | t_m(\mathbf{a}) | \mathbf{p}\sigma_1\sigma_2\alpha_1\alpha_2 \rangle. \end{aligned} \quad (2.12)$$

Reference [31] demonstrates in Sec. 2.3.2 that, despite the complex nature of the operators t_m and L_d and the explicit presence of the imaginary unity in Eq. (2.4), $\mathcal{E}_\mathcal{L}$ is real for the case of equal Fermi momenta. The demonstration is rather technical and we omit it here for brevity and to avoid repeating ourselves with Ref. [31]. The basic point is that the argument of the \ln in Eq. (2.4) can be diagonalized and its eigenvalues are phase factors of unite modulus. This is why the arctan series found in Refs. [21,22] always appear in these calculations.

C. Power counting

Reference [25] develops a low-energy power counting for nuclear matter, with the fermion-fermion interactions counted as $\mathcal{O}(1)$. Low-energy nucleon-nucleon interactions fall into this category because of their nonperturbative nature [26,37]. In this counting a fermion energy $\mathbf{p}^2/2m$ is counted as $\mathcal{O}(k_F^2)$, and then a fermion propagator as $\mathcal{O}(k_F^{-2})$, which also applies to a Fermi-sea insertion within an IGV. We denote by v_i the number of bosons (heavy and light) attached to the i th bilinear vertex, of which ω_i are heavy fields, and by d_i its number of derivatives. Concerning the purely bosonic vertices from \mathcal{L}_ϕ we denote by n_i the number of light fields in the i th vertex, and by δ_i the number of derivatives there. Finally, the total numbers of vertices from $\mathcal{L}_{\bar{\psi}\psi}$ and \mathcal{L}_ϕ are called V and V_π , respectively, and the total number of external light bosonic lines is called E_π .

With this preamble one can calculate straightforwardly the chiral dimension ν of an in-medium diagram, i.e., the power to which the typical size of the momentum involved in the diagram is raised. The original derivation can be found in Ref. [25], and is reviewed and simplified in Ref. [37]. The

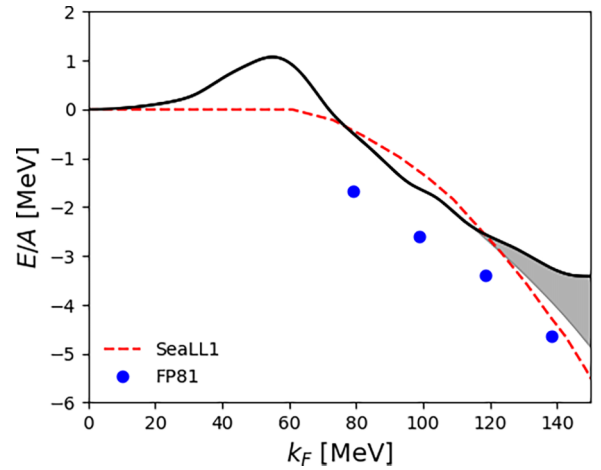


FIG. 2. The energy per nucleon for SNM as a function of $k_F < 150$ MeV from the ladder resummation is given by the black solid line, and the gray area represents the estimated uncertainty. In addition, we also show the results from the variational calculation of Ref. [52] (blue filled circles) and the density functional SeaLL1 [53] (red dashed line).

resulting expression for the power counting is

$$\begin{aligned} \nu &= 3 - E_\pi + \sum_{i=1}^{V_\pi} (\delta_i + n_i - 4) \\ &+ \sum_{i=1}^N (d_i + v_i + \omega_i - 2) + V_\rho. \end{aligned} \quad (2.13)$$

For the calculation of the interacting part of \mathcal{E} at least two fermions are involved in the interaction, so that $V_\rho \geq 2$, and there are no external light fields. Its leading-order (LO) contribution has $V_\rho = 2$ and chiral order $\nu = 5$. Higher order contributions arise by increasing V_ρ or any of the coefficients inside parentheses concerning the number of bosonic lines or derivatives, so that the combinations in parentheses become positive, instead of being zero as for the LO contributions.

Let us also notice that for small values of k_F , such that it is much smaller than the light-field masses, we can also consider the latter as heavy fields and run into the limit of only contact interactions. This is a limit of special significance for the applications developed below, and also for nuclear physics in general. Then, the power counting in Eq. (2.13) simplifies to

$$\nu = 3 + \sum_{i=1}^N (d_i + 2\omega_i - 2) + V_\rho. \quad (2.14)$$

Notice that the parenthesis is ≥ 0 as long as $d_i \geq 0$ because $\omega_i \geq 1$. The LO contributions to \mathcal{E} are those with $V_\rho = 2$ and vanishing combinations inside the parenthesis. In the applications discussed in Secs. V A and V B we actually go beyond the LO contributions because the vacuum nucleon-nucleon interactions are given in terms of their phenomenological phase shifts and mixing angles, despite in-medium corrections being implemented at LO by resumming the ladder diagrams.

A posteriori, by attending to the contribution of off-shell momenta above the pion mass to $\bar{\mathcal{E}}$ for SNM (cf. Fig. 2), we

deduce a value for the expansion scale Λ around 350 MeV. This number stems from having an uncertainty of 1.5 MeV for a value of $\tilde{\mathcal{E}}$ around -3.5 MeV at $k_F = 150$ MeV. Then, according to Eq. (2.14), the next-to-leading order (NLO) in-medium correction with $V_\rho = 3$ is suppressed by an extra power of k_F/Λ , from where $\Lambda \approx 350$ MeV results. An analogous procedure for PNM drives to a larger Λ ; cf. Fig. 5.

D. Partial-wave expansion

This subsection corresponds basically to Sec. 3 of Ref. [31], to which we refer for more details. The only addition here, which indeed is rather straightforward to implement, consists of taking into account the isospin degrees of freedom. Within the notation developed so far we can rewrite Eq. (2.4) as

$$\mathcal{E}_H = -i \int \frac{p dp}{m\pi} \int \frac{d^3 a}{\pi^3} \text{Tr} \{ \ln [I - t_m(\mathbf{a}) L_d(p, \mathbf{a})] \} \quad (2.15)$$

$$= -\frac{i}{2} \sum_{\sigma_{1,2}, \alpha_{1,2}} \int \frac{p dp}{m\pi} \int \frac{d^3 a}{\pi^3} \int \frac{d\hat{\mathbf{p}}}{4\pi} {}_A \langle \mathbf{p}, \sigma_1 \sigma_2 \alpha_1 \alpha_2 | \ln [I - t_m(\mathbf{a}) L_d(p, \mathbf{a})] | \mathbf{p}, \sigma_1 \sigma_2 \alpha_1 \alpha_2 \rangle_A. \quad (2.16)$$

An extra factor of 1/2 is introduced in the last equation due to the antisymmetrized nature of the two-fermion states, indicated by the subscript A in the bra and kets.

Another simplification in the expression for \mathcal{E}_L comes from rotational symmetry, so that one can take always \mathbf{a} along the $\hat{\mathbf{z}}$ axis. Next, we make a PWA expansion in the relative-motion variables \mathbf{p} in terms of the partial-wave vector states $|J\mu\ell SI i_3, p\rangle$, where J is the total angular momentum, μ is its third component, ℓ is the orbital angular momentum, S is the total spin, I is the total isospin, and i_3 is its third component. One has to take into account the value for the scalar product between a partial-wave vector $|J\mu\ell SI i_3 p\rangle$ and the plane-wave ones $|\mathbf{p}, \sigma_1 \sigma_2 \alpha_1 \alpha_2\rangle_A$. The relation between both bases is

$$\begin{aligned} |\mathbf{p}, \sigma_1 \sigma_2 \alpha_1 \alpha_2\rangle_A &= \sqrt{4\pi} \sum_{J\mu\ell S} (\sigma_1 \sigma_2 \sigma_3 |s_1 s_2 S) (m \sigma_3 \mu | \ell S J) (\alpha_1 \alpha_2 i_3 | \tau_1 \tau_2 I) Y_\ell^m(\hat{\mathbf{p}})^* \chi(S\ell I) |J\mu\ell SI i_3 p\rangle, \\ {}_A \langle \mathbf{p}', \sigma_1 \sigma_2 \alpha_1 \alpha_2 | J\mu\ell SI i_3 p\rangle &= \chi(S\ell) \frac{4\pi^{\frac{5}{2}} \delta(p' - p)}{p^2} (\sigma_1 \sigma_2 \sigma_3 |s_1 s_2 S) (m \sigma_3 \mu | \ell S J) (\alpha_1 \alpha_2 i_3 | \tau_1 \tau_2 I) Y_\ell^m(\hat{\mathbf{p}}), \\ \chi(S\ell I) &= \frac{1 - (-1)^{\ell+S+I}}{\sqrt{2}}. \end{aligned} \quad (2.17)$$

The factor $\chi(S\ell I)$ is nonzero for odd $\ell + S + I$, as required by Fermi statistics for a two-fermion state. After taking into account the standard orthogonality properties for the Clebsch-Gordan coefficients and spherical harmonics [38], one has

$$\mathcal{E}_L = -\frac{2i}{m\pi^3} \sum_{\substack{J, \mu, \ell \\ S, I, i_3}} \chi(S\ell I)^2 \int_0^\infty p dp \int_0^\infty a^2 da (J\mu\ell SI i_3 p | \ln [I - t_m(a\hat{\mathbf{z}}) L_d(p, a\hat{\mathbf{z}})] | J\mu\ell SI i_3 p). \quad (2.18)$$

Let us remark that the presence of $L_d(p, a\hat{\mathbf{z}})$ limits the possible values of a and p since it requires that $\xi_1^2 + \xi_2^2 \geq 2(a^2 + p^2) \geq 0$.

III. INTEGRAL EQUATIONS FOR $t_m(a\hat{\mathbf{z}})$

The vacuum T matrix t satisfies the Lippmann-Schwinger equation

$$t = V - VG(p)t, \quad (3.1)$$

where V is the potential and $G(p)$ is the vacuum unitarity loop function with intermediate states involving two fermions,

$$G(p) = -\frac{m}{2} \int \frac{d^3 k}{(2\pi)^3} \frac{|\mathbf{k}\rangle_A \langle \mathbf{k}|}{k^2 - p^2 - i\epsilon}. \quad (3.2)$$

Then, the operational equation Eq. (2.11) for $t_m(\mathbf{a})$ can also be expressed as [31]

$$t_m(\mathbf{a}) = V - V[G(p) - L_m(p, \mathbf{a})]t_m(\mathbf{a}) \quad (3.3)$$

for a given $E = p^2/m$. This operational relation straightforwardly drives to the following IE for the matrix elements of $t_m(\mathbf{a})$:

$$\begin{aligned} {}_A \langle \mathbf{p}' \sigma'_1 \sigma'_2 \alpha'_1 \alpha'_2 | t_m(\mathbf{a}) | \mathbf{p} \sigma_1 \sigma_2 \alpha_1 \alpha_2 \rangle_A &= {}_A \langle \mathbf{p}' \sigma'_1 \sigma'_2 \alpha'_1 \alpha'_2 | V | \mathbf{p} \sigma_1 \sigma_2 \alpha_1 \alpha_2 \rangle_A + \frac{m}{2} \sum_{\tilde{\sigma}, \tilde{\alpha}} \int \frac{d^3 k}{(2\pi)^3} {}_A \langle \mathbf{p}' \sigma'_1 \sigma'_2 \alpha'_1 \alpha'_2 | V | \mathbf{k} \tilde{\sigma}_1 \tilde{\sigma}_2 \tilde{\alpha}_1 \tilde{\alpha}_2 \rangle_A \\ &\times \frac{1 - \theta(\xi_{\tilde{\alpha}_1} - |\mathbf{k} + \mathbf{a}|) - \theta(\xi_{\tilde{\alpha}_2} - |\mathbf{k} - \mathbf{a}|)}{k^2 - p^2 - i\epsilon} {}_A \langle \mathbf{k} \tilde{\sigma}_1 \tilde{\sigma}_2 \tilde{\alpha}_1 \tilde{\alpha}_2 | t_m(\mathbf{a}) | \mathbf{p} \sigma_1 \sigma_2 \alpha_1 \alpha_2 \rangle_A. \end{aligned} \quad (3.4)$$

The matrix elements of the kernel $G(p) - L_m(p, \mathbf{a})$, used to deduce the previous equation, are worked out in Appendix A.

A. Integral equation for $t_m(a\hat{z})$ in partial waves: General values for ξ_1, ξ_2

Now, we give the integral equation for $t_m(a\hat{z})$ for general values of ξ_1 and ξ_2 , so that ξ_1 and ξ_2 are not assumed to be equal, as was the case in Ref. [31]. This generalization is only relevant for $i_3 = 0$, since for $i_3 = \pm 1$ then $\tilde{\alpha}_1 = \tilde{\alpha}_2 = \pm 1/2$, respectively, and for these cases one can take directly the result from Sec. 4 of Ref. [31].

The resulting IE in partial waves is

$$\begin{aligned} \langle J'\mu\ell'SI'i_3p'|t_m(a\hat{z})|J\mu\ell'SI'i_3p\rangle &= \langle J'\mu\ell'SI'i_3p'|V|J\mu\ell'SI'i_3p\rangle + m \sum_{\substack{J_1\ell_1m_3 \\ s_3\ell_2I_1}} \int \frac{d^3k}{(2\pi)^2} \frac{\chi(S\ell_2I')\chi(S\ell_1I_1)}{k^2 - p^2 - i\epsilon} \\ &\times (m_3s_3\mu|\ell_2SJ')(m_3s_3\mu|\ell_1SJ_1)Y_{\ell_2}^{m_3}(\hat{\mathbf{k}})^*Y_{\ell_1}^{m_3}(\hat{\mathbf{k}})\langle J'\mu\ell'SI'i_3p'|V|J'\mu\ell_2SI'i_3k\rangle \\ &\times \langle J_1\mu\ell_1SI_1i_3k|t_m(a\hat{z})|J\mu\ell'SI'i_3p\rangle\{1 - \theta(\xi_1 - |\mathbf{k} + a\hat{z}|) - \theta(\xi_2 - |\mathbf{k} - a\hat{z}|)\}. \end{aligned} \quad (3.5)$$

The necessary steps to end with this IE for PWAs from Eq. (3.4) for plane waves are derived in detail in Appendix A.

We can write the IE in Eq. (A14) in a more compact matrix form as

$$[t_m(a\hat{z})](p', p) = [V](p', p) + \frac{m}{(2\pi)^2} \int_0^\infty \frac{k^2 dk}{k^2 - p^2 - i\epsilon} [V](p', k) \mathcal{A}[t_m(a\hat{z})](k, p), \quad (3.6)$$

with the matrices

$$[V](p', k)_{J'\ell'I', J_2\ell_2I_2} = \delta_{J'J_2}\delta_{I'I_2}\langle J'\mu\ell'SI'i_3p'|V|J_2\mu\ell_2SI_2i_3k\rangle, \quad (3.7)$$

$$[t_m(a\hat{z})](k, p)_{J_1\ell_1I_1, J\ell I} = \langle J_1\mu\ell_1SI_1i_3k|t_m(a\hat{z})|J\mu\ell'SI'i_3p\rangle, \quad (3.8)$$

$$\begin{aligned} \mathcal{A}_{J_2\mu\ell_2I_2, J_1\mu\ell_1I_1} &= \chi(S\ell_2I_2)\chi(S\ell_1I_1) \sum_{m_3s_3} (m_3s_3\mu|\ell_2SJ_2)(m_3s_3\mu|\ell_1SJ_1) \int d\hat{\mathbf{k}} Y_{\ell_2}^{m_3}(\hat{\mathbf{k}})^* Y_{\ell_1}^{m_3}(\hat{\mathbf{k}}) \\ &\times \{1 - \theta(\xi_1 - |\mathbf{k} + a\hat{z}|) - \theta(\xi_2 - |\mathbf{k} - a\hat{z}|)\}. \end{aligned} \quad (3.9)$$

We also notice that our final expressions for the IE obeyed by $t_m(a\hat{z})$, Eqs. (3.5) and (3.9), are also applicable when $i_3 = \pm 1$ by just replacing

$$\theta(\xi_1 - |\mathbf{k} + a\hat{z}|) + \theta(\xi_2 - |\mathbf{k} - a\hat{z}|) \rightarrow 2\theta(\xi_{\frac{i_3}{2}} - |\mathbf{k} - a\hat{z}|), \quad (3.10)$$

which is the case studied in Ref. [31].

There are symmetry properties of the PWA matrix elements such that they are symmetric under the exchange of the initial and final states, and also there is a definite relation between the PWA matrix elements with opposite values of μ . These symmetry relations are stated and demonstrated in Appendix B.

IV. GENERAL SOLUTION OF THE PWAs FOR CONTACT INTERACTIONS

We consider the two-fermion scattering by a zero-range potential. We also adjust the normalization of the PWAs such that it is the same as in the ERE, that is, $\text{Im}t(p, p) = -p|t(p, p)|^2$. This choice is convenient since it simplifies the matching procedure with the ERE heavily used in the following. This implies multiplying by a factor $4\pi/m$ the PWAs from the previous sections.

A. The uncoupled case

We start with the LS equation in partial waves,

$$t(q, r) = v(q, r) - v(q, q')Gt(q', r), \quad (4.1)$$

where, to shorten the notation, we do not show the integration symbol over q' , nor the full integrand, all this being understood when this continuous variable is repeated. For instance, after including all the factors and symbols Eq. (4.1)

becomes

$$t(q, r) = v(q, r) + \frac{2}{\pi} \int_0^\infty \frac{q'^2 dq'}{q'^2 - p^2 - i\epsilon} v(q, q')t(q', r). \quad (4.2)$$

We now explicitly build in the momentum factors required by the centrifugal barrier potential, which factorize in PWAs for contact interactions without left-hand cut (LC). Thus, we write

$$\begin{aligned} t(q, q') &= q^\ell q'^\ell \tau_\ell(q^2, q'^2), \\ v(q, q') &= q^\ell q'^\ell w(q^2, q'^2), \end{aligned} \quad (4.3)$$

where $w(q^2, q'^2)$ is a polynomial in its arguments.³ As a result the LS equation becomes

$$\tau_\ell(q^2, r^2) = w(q^2, r^2) - w(q^2, q'^2)q'^{2\ell}G\tau_\ell(q'^2, r^2). \quad (4.4)$$

³The reduced potential function $w(q^2, q'^2)$ only depends on the square of the momenta because the full potential $q^\ell q'^\ell w(q^2, q'^2)$ under the exchange $q \rightarrow -q$ and $q' \rightarrow -q'$ scales as $(-1)^\ell$ and $(-1)^{\ell'}$, respectively [39]. This is accounted for by the prefactor $q^\ell q'^\ell$.

In order to calculate the on-shell T matrix in the medium we also need the off-shell T matrix in vacuum. An important remark to note in the IE for $t_m(q, p)$, Eq. (2.12), is that the off-shell momenta are bounded because the intermediate states are of an in-medium mixed type, contributing to the loop integral L_m of one baryon line inside the Fermi sea; cf. Eq. (2.9). Furthermore, once the on-shell $t_m(\mathbf{p}, \mathbf{p}, \mathbf{a})$ is calculated the momenta involved in Eq. (2.18) for evaluating \mathcal{E} are bounded by the Fermi momenta because of L_d . Therefore, q/Λ and p/Λ vanish for $\Lambda \rightarrow \infty$, in both the off- and on-shell cases, respectively. Let us notice that this is not the case in *vacuum*, because when working out the off-shell T matrix from a LS equation one must consider off-shell momenta as large as the cutoff.

We first consider half-off-shell scattering, and afterwards we generalize our analysis to the off-shell case. Due to half-off-shell unitarity in partial waves (see, e.g., Sec. 2 of Ref. [39]), we can write the PWA as

$$\tau_\ell(q^2, p^2) = D^{-1}(p^2)N(q^2, p^2), \quad (4.5)$$

Since there is no LC for a zero-range potential then $N(q^2, q'^2)$ is a rational function in its arguments, being real for real momenta [40]. Here, $D(p^2)$ is an analytic function in the cut complex p^2 plane with only a right-hand cut (RHC) for real and positive values of p^2 .

For on-shell scattering $q^2 = q'^2 = p^2$ and we can reabsorb $N(p^2, p^2)$ in a redefinition of $D(p^2)$, such that [40]

$$N(p^2, p^2) = 1. \quad (4.6)$$

To achieve this just divide the original numerator and denominator functions in $\tau_\ell(p^2, q'^2)$ by $N(p^2, p^2)$. The possible zeros of $N(p^2, p^2)$ would give rise to poles in the function $D(p^2)$: the Castillejo-Dalitz-Dyson poles [40,41].

Adopting in the following the convenient redefinition in Eq. (4.6), the imaginary part of $D(p^2)$ along the RHC becomes

$$\text{Im } D(p^2) = -p^{2\ell} \sqrt{p^2}, \quad p^2 > 0. \quad (4.7)$$

Implementing Eq. (4.5) into Eq. (4.4), one deduces from the latter the following IE for $N(q^2, p^2)$:

$$N(q^2, p^2) = D(p^2)w(q^2, p^2) - w(q^2, q'^2)q'^{2\ell} \mathfrak{R}GN(q^2, p^2), \quad (4.8)$$

The imaginary part of this equation is zero because of Eq. (4.7), taking into account that $\text{Im } G = -p$. This is indeed a consistency check of the general result that $N(q^2, p^2)$ has no RHC. Denoting the real part of $D(p^2)$ by $D_r(p^2)$, Eq. (4.8) becomes

$$\begin{aligned} N(q^2, p^2) &= D_r(p^2)w(q^2, p^2) - w(q^2, q'^2)q'^{2\ell} \mathfrak{R}GN(q^2, p^2) \\ &= D_r(p^2)w(q^2, p^2) + Q(q^2, p^2), \end{aligned} \quad (4.9)$$

with

$$Q(q^2, p^2) = -w(q^2, q'^2)q'^{2\ell} \mathfrak{R}GN(q^2, p^2), \quad (4.10)$$

which is a polynomial in the q^2 argument. Notice that $q'^{2\ell} \mathfrak{R}G$ is meant to represent the Cauchy principal part of the q' integral involved.

To shorten the notation when considering on-shell scattering, the different functions τ_ℓ , Q , and w are written with only one argument, namely, as $\tau_\ell(p^2)$, $Q(p^2)$, and $w(p^2)$, respectively. For on-shell scattering, in which $N(p^2) = 1$, we can isolate $D_r(p^2)$ from Eq. (4.9), which then reads

$$D_r(p^2) = \frac{1 - Q(p^2)}{w(p^2)}. \quad (4.11)$$

This function is the one that is matched with the ERE,

$$D_r(p^2) = -\frac{1}{a} + \frac{1}{2}rp^2 + \sum_{m=2}^{\infty} v_m p^{2m} = p^{2\ell+1} \cot \delta_\ell. \quad (4.12)$$

Let us stress that this result is a consequence of unitarity and analyticity, with the latter exploiting the fact that no LC is present in the PWAs when considering only contact interactions. It is entirely expressed in terms of the experimental phase shifts.

To calculate $N(q^2, p^2)$ we substitute the expression for $D_r(p^2)$, Eq. (4.11), into Eq. (4.9), which then reads

$$N(q^2, p^2) = \frac{w(q^2, p^2)}{w(p^2)} + Q(q^2, p^2) - Q(p^2) \frac{w(q^2, p^2)}{w(p^2)}. \quad (4.13)$$

By solving explicit examples of off-shell scattering with cutoff regularization for contact interactions with the potential $w(q'^2, q'^2) = \sum_{\alpha, \beta=0} \omega_{\alpha\beta} q'^{2\alpha} q'^{2\beta}$ up to and including sixth degree in the arguments, we have checked that, after renormalization by matching with the ERE,⁴ the coefficients $\omega_{\alpha\beta}$ scale with the cutoff Λ as

$$\omega_{\alpha\beta} \xrightarrow{\Lambda \rightarrow \infty} O(\Lambda^{-2(\alpha+\beta)}). \quad (4.14)$$

This rule follows the dimension of $\omega_{\alpha\beta}$ corresponding to $\text{length}^{2(\alpha+\beta)+1}$, and we take it for granted in the following discussions. The previous equation also holds for a separable potential.⁵

Importantly, Eq. (4.14) allows one to conclude that

$$N(q^2, p^2) \xrightarrow{\Lambda \rightarrow \infty} 1. \quad (4.15)$$

The reasoning is the following: (i) The ratio $w(q^2, p^2)/w(p^2) \rightarrow \omega_{00}/\omega_{00} = 1$ for $\Lambda \rightarrow \infty$, and then Eq. (4.13) simplifies as

$$N(q^2, p^2) = 1 + Q(q^2, p^2) - Q(p^2). \quad (4.16)$$

(ii) The monomial $\omega_{\alpha\beta}(q^2, q'^2)$ gives rise to extra cutoff powers of highest power $\Lambda^{2\beta}$ when implemented in the IE

⁴The divergent part of the integrals involved can be expressed in terms of the basic functions

$$I_n = \frac{2}{\pi} \int_0^\Lambda \frac{q^2 dq}{q^2 - p^2} q^{2n} = \int_0^\Lambda dq q^{2n} + p^2 I_{n-1},$$

$$L_n = \frac{2}{\pi} \int_0^\Lambda dq q^{2n} = \theta_n \Lambda^{2n+1}.$$

The coefficients θ_n specify the cutoff regularization scheme.

⁵An explicit account of our analyses with contact-interaction potentials can be provided to the interested reader on demand.

Eq. (4.4), as compared with those stemming from ω_{00} . However, the latter, because of its dimension ruling the scaling with the cutoff, is less suppressed precisely by $\mathcal{O}(\Lambda^{-2(\alpha+\beta)})^\ell$ as compared with $w_{\alpha\beta}$. Therefore, even taking into account the extra cutoff powers resulting by integrating the off-shell arguments in the IE of τ_ℓ , it comes out that the contributions to this IE from $w_{\alpha\beta}$ are suppressed by $\mathcal{O}(\Lambda^{-2\alpha})$ for $\alpha > 0$, as compared to those from ω_{00} . Therefore, the contribution with $\alpha > 0$ vanishes in $Q(q^2, p^2)$ for $\Lambda \rightarrow \infty$.

However, for $\alpha = 0$ there is no such suppression of the contributions arising from the integration of $w_{0\beta}(q^2, q'^2)$ to the left of the symbol $\Re G$ in Eq. (4.10). In the same manner, when the potential $w(q'^2, p^2)$ acts to the right in Eq. (4.10) (think of an iterative solution of this IE), the only surviving contributions in the limit $\Lambda \rightarrow \infty$ correspond to $\omega_{\beta 0}$. Importantly, all these contributions involving $\omega_{0\alpha}$ to the left or $\omega_{\beta 0}$ to the right of $\Re G$ in Eq. (4.10) are independent of q , because the integration in the q' variable is then only a function of p^2 . Thus, they cancel in the difference $Q(q^2, p^2) - Q(p^2)$ present in Eq. (4.16), and Eq. (4.15) follows.

For the off-shell case one writes $\tau_\ell(q^2, r^2) = D^{-1}(p^2)N(q^2, r^2)$, with r another momentum, substitutes it in Eq. (4.4) and, by taking into account the scaling rule of Eq. (4.14), one has that

$$N(q^2, r^2) = D(p^2)\omega_{00} - w(q^2, q'^2)q'^{2\ell}GN(q'^2, r^2). \quad (4.17)$$

This equation has no imaginary part because of Eqs. (4.7) and (4.15) [due to time-reversal invariance $N(p^2, q^2) = N(q^2, p^2)$], and then $N(q^2, r^2)$ has no RHC. Therefore, $N(q^2, r^2)$ satisfies an equation analogous to Eq. (4.16),

$$N(q^2, r^2) = 1 + Q(q^2, r^2) - Q(p^2). \quad (4.18)$$

Following then the same reasoning as used below Eq. (4.16), one concludes that

$$N(q^2, q'^2) \xrightarrow{\Lambda \rightarrow \infty} 1. \quad (4.19)$$

As a consequence of Eqs. (4.5), (4.12), and (4.19), the vacuum off-shell PWAs can be expressed directly in terms of the experimental phase shifts for $q, q' \leq 2\max(\xi_1, \xi_2)$ as

$$t(q, q') = \frac{(qq')^\ell}{p^{2\ell+1} \cot \delta_\ell - ip^{2\ell+1}}. \quad (4.20)$$

B. The coupled case

This section is a generalization to coupled PWAs of the results in Sec. IV A, and we follow similar steps as in the uncoupled case. We use matrix notation which makes more straightforward this generalization process. For M coupled PWAs the LS equation in matrix notation is written as

$$t(q, r) = v(q, r) - v(q, q')Gt(q', r), \quad (4.21)$$

so that now t and v are $M \times M$ matrices and G is a diagonal matrix of the same order. We also introduce the matrix $(q)^\ell$ which is a diagonal matrix whose i th entry is q^{ℓ_i} , being ℓ_i the orbital angular momentum of the i th PWA. The right threshold behaviors of $t(q, q')$ and $v(q, q')$ are explicitly taken into

account analogously to Eq. (4.3) by writing, respectively,

$$\begin{aligned} t(q, q') &= (q)^\ell \tau_\ell(q^2, q'^2)(q')^\ell, \\ v(q, q') &= (q)^\ell w(q^2, q'^2)(q')^\ell. \end{aligned} \quad (4.22)$$

Multiplying Eq. (4.21) by $(q)^{-\ell}$ and $(q')^{-\ell}$ to the left and right, respectively, we have

$$\tau_\ell(q^2, r^2) = w(q^2, r^2) - w(q^2, q'^2)(q')^{2\ell}G\tau_\ell(q'^2, r^2). \quad (4.23)$$

Invoking the N/D method in coupled channels [42], we write

$$\begin{aligned} \tau_\ell(q^2, q'^2) &= N(q^2, q'^2)D^{-1}(p^2), \\ \text{Im } D(p^2) &= -(p)^{2\ell+1}N(p^2), \end{aligned} \quad (4.24)$$

where $D(p^2)$ and $N(q^2, q'^2)$ are $M \times M$ matrices. The former has only RHC and the latter has none in the case of contact interactions. Both matrices of functions can be chosen such that for on-shell scattering [40]

$$N(p^2) = \mathbb{I}. \quad (4.25)$$

The equation for $N(q^2, r^2)$ that results from Eq. (4.23) is

$$N(q^2, r^2) = w(q^2, r^2)D(p^2) - w(q^2, q'^2)(q')^{2\ell}GN(q'^2, r^2). \quad (4.26)$$

Particularizing this equation to on-shell scattering we have that

$$D_r(p^2) = w(p^2)^{-1}[\mathbb{I} - Q(p^2)], \quad (4.27)$$

where $D_r(p^2) = \Re D(p^2)$ and

$$Q(q^2, r^2) = -w(q^2, q'^2)(q')^{2\ell}\Re GN(q'^2, r^2). \quad (4.28)$$

Equation (4.27) is matched with the ERE in coupled channels to all orders, so that

$$\begin{aligned} D_r(p^2) &= w(p^2)^{-1}(\mathbb{I} - Q(p^2)) \\ &= -(a)^{-1} + \frac{1}{2}(r)p^2 + \sum_{m=2}^{\infty} (v_m)p^{2m}. \end{aligned} \quad (4.29)$$

Here all the shape parameters are actually matrices [43], a fact indicated by placing them between brackets.

Explicitly, if $S(p^2)$ is the S -matrix projected in partial waves, the corresponding coupled PWAs can be written as

$$t(p^2) = (p)^\ell D^{-1}(p^2)(p)^\ell = \frac{1}{2ip}[S(p^2) - \mathbb{I}]. \quad (4.30)$$

For vacuum NN scattering, the S matrix for coupled PWAs can be expressed as

$$S = \begin{pmatrix} \cos 2\epsilon e^{2\delta_1} & i \sin 2\epsilon e^{i(\delta_1+\delta_2)} \\ i \sin 2\epsilon e^{i(\delta_1+\delta_2)} & \cos 2\epsilon e^{2i\delta_2} \end{pmatrix}, \quad (4.31)$$

where ϵ is the mixing angle and δ_{11}, δ_{22} are the phase shifts for waves 1 and 2, respectively.

A completely analogous analysis as for the single-channel case implies that $N(q^2, q'^2) \rightarrow \mathbb{I}$ for $\Lambda \rightarrow \infty$ (we recall that we are interested in off-shell momenta bounded by twice the

largest Fermi momentum). Therefore, when the cutoff is sent to infinity, the expression for the off-shell coupled PWAs is

$$t(q, q') = \left(\frac{q}{p}\right)^\ell \frac{1}{2ip} (S(p^2) - \mathbb{I}) \left(\frac{q'}{p}\right)^\ell. \quad (4.32)$$

In the previous expression the matrix $(q/p)^\ell$ is $(q)^\ell (p)^{-\ell} = (p)^{-\ell} (q)^\ell$. As in the uncoupled case, Eq. (4.32) has been checked for polynomial potentials in coupled channels up to sixth degree in its arguments.

C. The in-medium T matrix

For the in-medium T matrix the results for the vacuum T matrix expressed in Eqs. (4.20) and (4.32) allow us to derive an algebraic equation to determine $t_m(q, p)$. We explicitly take care of the threshold behavior for interactions without LC, and write

$$t_m(q, q') = (q)^\ell \tau_m(p^2) (q')^\ell, \quad (4.33)$$

Of course, for coupled PWAs a matrix notation analogous to that developed in Sec. IV B should be understood.

Next, by taking into account the IE satisfied by t_m , Eq. (2.11), it follows that τ_m obeys the *algebraic* matrix equation,

$$\tau_m(p^2) = \tau_\ell(p^2) + \tau_m(p^2) q'^\ell L_m q'^{\ell'} \tau_\ell(p^2), \quad (4.34)$$

with the matrix elements of $q'^\ell L_m q'^{\ell'}$ given by

$$\begin{aligned} & [q'^\ell L_{m; J_2 \mu_2 \ell_2, J_1 \mu_1 \ell_1} q'^{\ell'}]_{J_2 \ell_2, J_1 \ell_1} \\ &= \delta_{\mu_2 \mu_1} \frac{m}{(2\pi)^2} \int_0^\infty \frac{k^2 dk}{k^2 - p^2 - i\epsilon} k^{\ell_1 + \ell_2} \mathcal{B}_{J_2 \mu_1 \ell_2 J_2, J_1 \mu_1 \ell_1 I_1}. \end{aligned} \quad (4.35)$$

The matrix $[\mathcal{B}]$ is given by the matrix $[\mathcal{A}]$, defined in Eq. (3.9), but removing the one in the factor between square brackets. Namely,

$$\begin{aligned} \mathcal{B}_{J_2 \mu_2 \ell_2 J_2, J_1 \mu_1 \ell_1 I_1} &= -\chi(S\ell_2 I_2) \chi(S\ell_1 I_1) \sum_{m_3 s_3} (m_3 s_3 \mu | \ell_2 S J_2) \\ &\times (m_3 s_3 \mu | \ell_1 S J_1) \int d\hat{\mathbf{k}} Y_{\ell_2}^{m_3}(\hat{\mathbf{k}}) Y_{\ell_1}^{m_3}(\hat{\mathbf{k}}) \\ &\times [\theta(\xi_1 - |\mathbf{k} + a\hat{\mathbf{z}}|) + \theta(\xi_2 - |\mathbf{k} - a\hat{\mathbf{z}}|)]. \end{aligned} \quad (4.36)$$

Finally, the solution of Eq. (4.34) is

$$\begin{aligned} \tau_m(p^2) &= [\tau_\ell(p^2)^{-1} - q'^\ell L_m q'^{\ell'}]^{-1} \\ &= \left[(p)^\ell \left(\frac{2\pi(S_\ell - \mathbb{I})}{imp} \right)^{-1} (p)^\ell - q'^\ell L_m q'^{\ell'} \right]^{-1}. \end{aligned} \quad (4.37)$$

D. Uniqueness of the on-shell in-medium T matrix

We discuss here that the *on-shell in-medium PWA* $t_m(p, a\hat{\mathbf{z}})$ shown in Eqs. (4.33) and (4.37) is independent of the regulator, as well as unique. The point is to consider the scattering amplitude of two on-shell fermions in the medium, whose

imaginary part is not only due to G but also to L_m . The former comprises the contributions from intermediate states of two fermions in vacuum, and the latter from the mixed intermediate states with one Fermi-sea insertion. As a result, $\tau_m(p^2)^{-1} - i(p)^\ell \text{Im}[G(p) - L_m](p)^\ell$ is amenable to a power expansion in p^2 around threshold because the branch-point singularity at $p = 0$ has been removed. This is then the in-medium equivalent of the ERE in vacuum; cf. Eq. (4.29).

From this point of view, this in-medium ERE can be seen as a dressing or flow of the ERE parameters in vacuum because of the finite density of fermions, so that one has $a(\xi_1, \xi_2)$, $r(\xi_1, \xi_2)$, and $v_m(\xi_1, \xi_2)$ for $m \geq 2$. In the limit $\xi_i \rightarrow 0$, of course, one has the boundary conditions $a(0, 0) = a$, $r(0, 0) = r$ and, in general, $v_m(0, 0) = v_m$, $m \geq 2$, where the vacuum values have been denoted with the usual symbols.

By using cutoff regularization we have been able to work out the dressing of the ERE parameters as a function of the Fermi momenta ξ_i . This is accomplished because $t_m(p, a\hat{\mathbf{z}})$ has been calculated to all orders in the ERE, being expressed directly in terms of the vacuum phase shifts and mixing angles. Since any other regularization method respecting analyticity and unitarity in the limit of contact interactions should agree on the on-shell $t_m(p, a\hat{\mathbf{z}})$ when taking into account all higher orders in the ERE, then it follows our claim.

Making use of these results, one can then resolve the regulator dependence [23] already observed of in-medium nonperturbative calculations of $\bar{\mathcal{E}}$ by performing them either with cutoff or dimensional regularization. The point here is not to perform partial calculations up to some order in the expansion of the contact interactions but to include all orders, so that the physical results are directly expressed in terms of the phase shifts and mixing angles as determined in vacuum scattering experiments.

V. RESULTS

We have resummed the ladder diagrams for calculating $\bar{\mathcal{E}}$, Eqs. (2.4) and (2.18). We have also been able to solve t_m in the nuclear medium for contact interactions; cf. Eqs. (4.33) and (4.37). As a consequence, our results are renormalized and expressed directly in terms of the experimental phase shifts and mixing angles of NN scattering [43].

The calculations are based on assuming contact interactions between the two interacting nucleons, whose range of validity is limited by the onset of the left-hand cut in PWAs due to pion exchanges, which occurs for $p^2 < -m_\pi^2/4$ (this limit is determined by one-pion exchange). Nonetheless, the on-shell PWAs in vacuum have been directly expressed in terms of the phase shifts, which is valid for all momenta. But the off-shell vacuum PWAs $t_{ij}(q, r)$, needed for in-medium calculations, are proportional to $q^{\ell_i} r^{\ell_j}$ in the off-shell momenta, a functional form stemming from the contact-interaction nature assumed for the potential. Indeed, one would expect this functional form to be valid only for small momentum compared with m_π . As said, $-m_\pi^2/4$ settles the start of the LC in the momentum-squared complex plane, so that the off-shell factor $q^{\ell_i} r^{\ell_j}$ would set in only as the limiting behavior for $|q|, |r| \ll m_\pi$. Therefore, we would expect that the strong off-shell dependence proportional to $k^{\ell_1 + \ell_2}$ in the

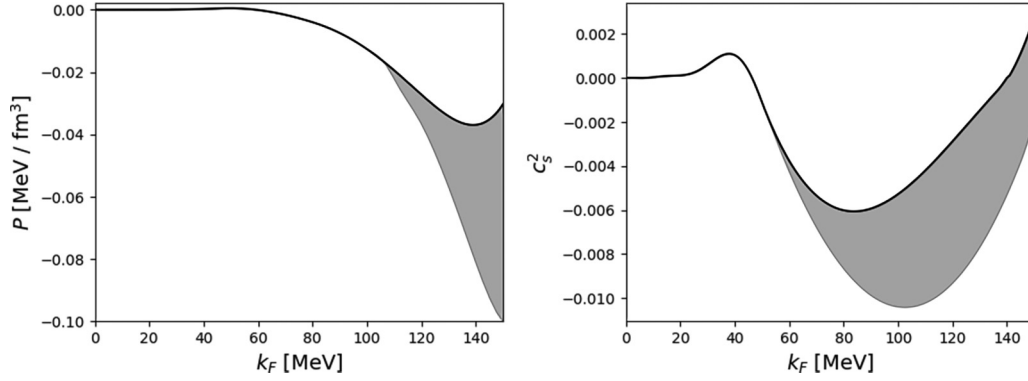


FIG. 3. The pressure (left panel) and sound velocity squared (right panel) for SNM calculated from the ladder resummation are plotted as functions of $k_F < 150$ MeV by the solid lines, with the estimated uncertainty given by the gray bands.

calculation of L_m in Eq. (4.35) would be tamed for momenta of $\mathcal{O}(m_\pi)$. For instance, this is the case if one calculates the NN PWAs at tree level from one-pion exchange, as given in Appendix A of [37].

Then, we display our results for low densities up to Fermi momenta $k_F = 150$ MeV $\sim m_\pi$, which corresponds to symmetric nuclear matter (SNM) and pure neutron matter (PNM) densities of 3×10^{-2} and 1.5×10^{-2} fm $^{-3}$, respectively. We notice that the onset of the sensitivity to the pion LC is smooth and gradual, as shown by the validity of the ERE with a few terms in reproducing the NN phase shifts for momenta clearly above $m_\pi/2$ [39,44–46]. Furthermore, here the use of the vacuum off-shell PWAs is always in integral expressions, so that there is an averaging process, and results are not directly sensitive to specific values of momenta. Then, we consider it reasonable to extrapolate in k_F and show the results for Fermi momenta up to around m_π . Indeed, it is not uncommon for pionless EFT to show results for momenta up to around m_π [47–49].

To estimate the uncertainty in this extrapolation, we also multiply the off-shell dependence on k for $k > m_\pi/2$ in the calculation of L_m , Eq. (4.35), by the Gaussian regulator $\exp[-(k - m_\pi/2)^2/Q^2]$. The scale $Q > m_\pi$, and in this way higher values of k compared with $m_\pi/2$ are suppressed in the calculation of L_m (the onset of LC in the complex k plane occurs at $\pm im_\pi/2$). Notice that this procedure is implemented only for estimating uncertainties, and our benchmark values correspond to $Q \rightarrow \infty$. The extent of the uncertainty is determined by taking the lowest value $Q = m_\pi$.

We also consider the impact in our results of taking an effective nucleon mass $m(\rho)$ in the nuclear medium. At the level of the kinetic energy density \mathcal{E}_K we have to replace m by $m(\rho)$ in Eq. (2.5). For the interacting energy density, \mathcal{E}_L , the substitution $m \rightarrow m(\rho)$ has to be made in L_m and L_d , but not in the calculation of the vacuum scattering PWA and, therefore, not in $(p)^\ell (\frac{2\pi(S_t - \mathbb{I})}{imp})^{-1} (p)^\ell$ for $\tau_m(p^2)$, Eq. (4.37). The replacement $m \rightarrow m(\rho)$ is also needed in the prefactor $-2i/(m\pi^3)$ in Eq. (2.18), since this is linked to the calculation of L_d . At nuclear matter saturation density ρ_0 Ref. [50] gives $m^* \equiv m(\rho_0) \approx 0.7m$, while for pure neutron matter Ref. [51] obtains $m^* \approx 0.9m$. We take these values and use for each case an extrapolation in density of the

form $m(\rho) = \frac{m}{1 + \frac{\rho}{\rho_0} (\frac{m^*}{m} - 1)}$ which becomes linear in ρ for low densities. This behavior is in agreement with Refs. [50,51], and it is also the expected leading one by having into account the self-energy corrections from NN interactions [20,25,26]. Nonetheless, this source of estimated uncertainty is typically much smaller than the one stemming from the variation of the Gaussian cutoff Q , and it is not really relevant in the presentation of our results.

A. Symmetric nuclear matter

We show in Fig. 2 the resulting $\bar{\mathcal{E}}$ from the ladder resummation as a function of k_F by the solid black line, and the estimated uncertainty corresponds to the gray area. In the same figure we also show other low-density determinations by the blue filled circles, corresponding to the variational calculation of Ref. [52], and the red dashed line is the result from the density functional SeaLL1 [53].

It is notorious that $\bar{\mathcal{E}} > 0$ up to $k_F \simeq 70$ MeV, or $\rho \simeq 3 \times 10^{-3}$ fm $^{-3}$. This clearly indicates that SNM is not stable at such low values of the density, where the resummation of the ladder diagrams provides robust results. Of course, this phenomenon should not come as a surprise since it is well known [54–56] that at low densities the stable phase is not longer homogeneous, as α particles [55,56] and heavy nuclei [54,55] form.

We can further study this region of instability of SNM, also called spinodial region [57], by considering the resulting pressure, P , and the sound velocity squared, c_s^2 , which respectively obey the expressions

$$P(\rho) = \rho^2 \frac{\partial \bar{\mathcal{E}}}{\partial \rho}, \quad (5.1)$$

$$c_s^2(\rho) = \frac{1}{m} \frac{\partial P}{\partial \rho} = \frac{2\rho}{m} \frac{\partial \bar{\mathcal{E}}}{\partial \rho} + \frac{\rho^2}{m} \frac{\partial^2 \bar{\mathcal{E}}}{\partial \rho^2}. \quad (5.2)$$

$P(\rho)$ and $c_s^2(\rho)$ are shown in the left panel and right panels of Fig. 3, respectively. The pressure is positive up to $k_F = 59$ MeV, corresponding to a system which tends to split apart. c_s^2 becomes positive in the region of negative $P(\rho)$ only above a critical value of k_F , which we denote as ξ_c , and for which the resummation of ladder diagrams yields $\xi_c = 139$ MeV, with

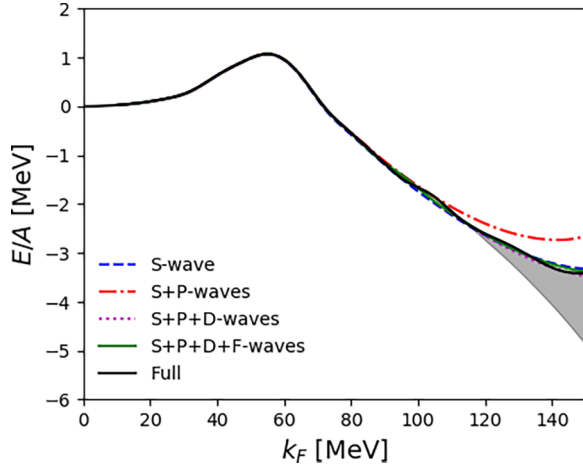


FIG. 4. The partial-wave contributions to $\bar{\mathcal{E}}$ for SNM with different orbital angular momenta are added separately. Contributions with the S , P , D , and F waves consecutively added correspond to the blue dashed, red dashed-dotted, magenta dotted, and green solid lines, respectively. The full result is the black solid line. See the text for further details.

around a +20 MeV of uncertainty. Let us recall the relation between the compressibility coefficient K and c_s^2 ,

$$K = \frac{c_s^2}{m\rho}, \quad (5.3)$$

so that when $c_s^2 < 0$ then $K < 0$. The Fermi momentum ξ_c is the critical density above which the system leaves the instability region, and SNM becomes a homogeneous stable phase. Reference [54], employing a relativistic mean field theory, obtained a value for the critical density around 10^{14} g/cm³, corresponding to $\xi_c = 190$ MeV. The boson-exchange model for nuclear interactions used to apply the Dirac-Bruckner approach to calculate $\bar{\mathcal{E}}$ in Ref. [57] gives $\xi_c \approx 200$ MeV.

We separately show in Fig. 4 the contributions from PWAs involving different orbital angular momenta, and their sum up to the final result given by the black solid line. We organize the different contributions according to the mixing of PWAs in vacuum. In this way, the blue dashed line corresponds to the S waves but, because of the mixing between the 3S_1 and 3D_1 PWAs, we are actually keeping the 1S_0 and 3S_1 - 3D_1 PWAs. Let us recall that we directly take the experimental phase shifts and mixing angles, so that the mixed PWAs in vacuum must be kept together. Similarly, using the notation of P waves (red dash-dotted line) we are adding the PWAs 1P_1 , 3P_0 , 3P_1 , 3P_2 - 3F_2 . For the D waves (magenta dotted line) we have in addition 1D_2 , 3D_2 , 3D_3 - 3G_3 , and for the F waves (green solid line) we have added the contributions from the 1F_3 , 3F_3 , and 3F_4 - 3H_4 PWAs. As expected, we see from Fig. 4 that the main contributions arise from the S waves, but the P waves give a noticeable repulsion, which is compensated to large extent by the D -wave contributions. The convergence is already achieved with the F -wave contributions, and is almost indistinguishable from the final curve including the G waves.

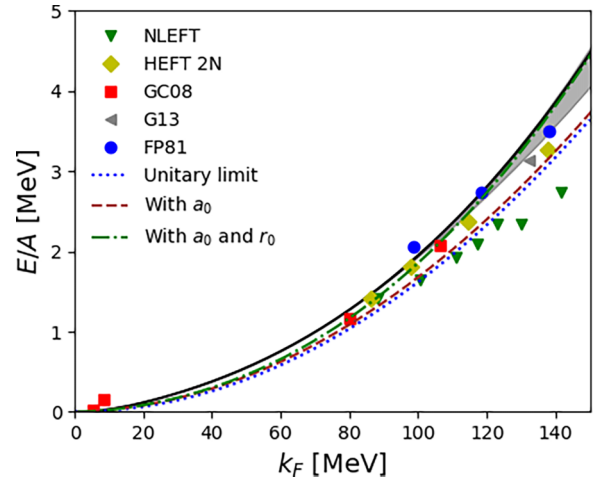


FIG. 5. $\bar{\mathcal{E}}$ for PNM is plotted as a function of $k_F < 150$ MeV. Our results are given by the black solid line, together with the gray band giving the uncertainty estimated. The resulting curve in the unitary limit $a_0 = \infty$ is the blue dotted line. We also provide the results calculated with the 1S_0 scattering length only, brown dashed line, plus the effective range, green dash-dotted line [31]. For comparison we show results for NLEFT [58] (green downwards triangles), HEFT 2N [59] (yellowish green diamonds), the two quantum Monte Carlo calculations of Gezerlis and Carlson [60] (red squares) and Gezerlis [61] (gray left-pointing triangles), as well as the variational one of Ref. [52] (blue circles).

B. Pure neutron matter

The results for $\bar{\mathcal{E}}$ of PNM by resumming the ladder diagrams are shown in Fig. 5 by the solid line, with an estimated uncertainty given by the gray band. By considering only the S -wave contributions, namely the PWA 1S_0 , we plot $\bar{\mathcal{E}}$ in the unitary limit (infinite scattering length) by the blue dotted line. When taking the actual value for the scattering length of the PWA 1S_0 , $a_0 = -18.95$ fm, the brown dashed line results and, after the effective-range contributions are added with $r_0 = 2.75$ fm, we have the green dot-dashed line. The last two cases were already calculated by us in Ref. [31]. In addition we also compare with other calculations. The green downwards triangles give the low-density results from nuclear lattice EFT of Ref. [58], and the blue filled circles correspond to the variational calculation of Ref. [52]. We also show the quantum Monte Carlo results of Refs. [60] (red squares) and [61] (gray left-pointing triangles) and the auxiliary-field quantum Monte Carlo calculation of [59] (light green diamonds). We see that $\bar{\mathcal{E}}$ for PNM obtained from the resummation of the ladder diagrams is more repulsive than any of the other calculations shown for $k_F \gtrsim 120$ MeV.

We also plot the pressure P and the sound velocity squared c_s^2 for PNM that result from the resummation of the ladder diagrams in the left and right panels of Fig. 6, respectively, with the gray bands giving the estimated uncertainty as discussed above.

Separated partial-wave contributions to $\bar{\mathcal{E}}$ for PNM are shown in Fig. 7, similarly to Fig. 4 for the case of SNM. Then, by S waves (blue dashed line) we mean the contributions from the 1S_0 PWA; P waves (red dotted line) comprise in addition

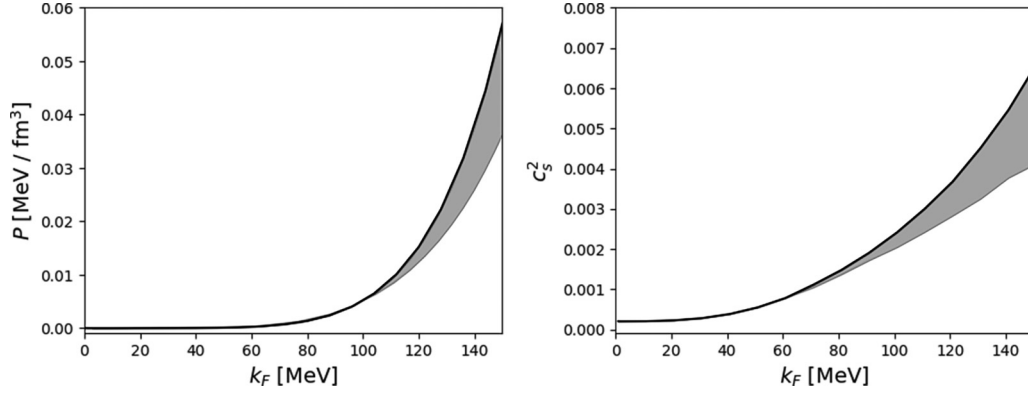


FIG. 6. The pressure $P(\rho)$ (left panel) and sound velocity squared $c_s^2(\rho)$ (right panel) that result from the ladder resummation for PNM are plotted by the solid lines.

those from 3P_0 , 3P_1 , and 3P_2 - 3F_2 ; D waves (magenta dash-dotted) include 1D_2 ; and F waves (green solid line) comprise the contributions from the 3F_3 and 3F_4 - 3H_4 PWAs. In the interval of values of k_F shown it is clear that the full result (black solid line) is overwhelmingly dominated by the 1S_0 PWA, with a small repulsive P -wave contribution, which is compensated by the D and higher partial waves. The convergence with the full result is reached with almost indistinguishable F -wave contributions.

By assuming a quadratic dependence of $\bar{\mathcal{E}}$ on the proton fraction $x_p \equiv \rho_p/\rho$ (with ρ_p the density of protons), we can calculate from our results the symmetry energy $S(\rho)$ as [28]

$$S(\rho) = \bar{\mathcal{E}}(\rho, 0) - \bar{\mathcal{E}}(\rho, \frac{1}{2}). \quad (5.4)$$

Here, we follow the notation $\bar{\mathcal{E}}(\rho, x_p)$ for $\bar{\mathcal{E}}$ as a function of density and proton fraction, so that $\bar{\mathcal{E}}(\rho, \frac{1}{2})$ corresponds to SNM and $\bar{\mathcal{E}}(\rho, 0)$ corresponds to PNM. Note that, in order to apply Eq. (5.4), one is taking the difference of energies per nucleon at a fixed value of density ρ . Then, k_F for SNM is a

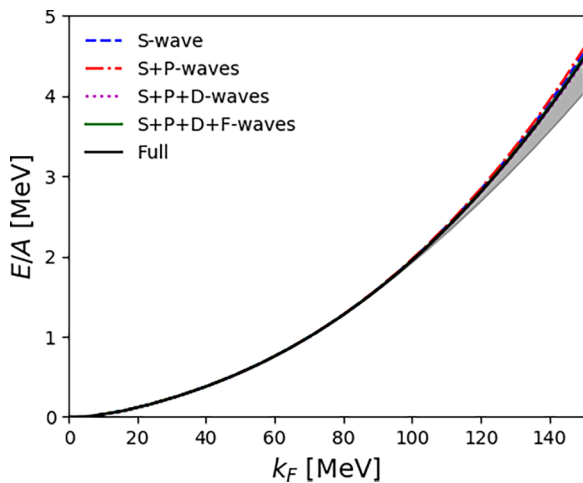


FIG. 7. The partial-wave contributions to $\bar{\mathcal{E}}$ for PNM with different orbital angular momenta are added separately. The notation is the same as that employed in Fig. 4 for SNM.

factor $1/2^{1/3}$ smaller than k_F for PNM when calculating the difference $S(\rho) = \bar{\mathcal{E}}(\rho, 0) - \bar{\mathcal{E}}(\rho, 0)$. From our results shown in Figs. 5 and 2 for PNM and SNM, respectively, we calculate $S(\rho)$, which is plotted in Fig. 8 by the solid line, with the gray area giving the uncertainty estimated.

Going on with the quadratic dependence on the proton fraction for $\bar{\mathcal{E}}(\rho, x_p)$, Ref. [62] wrote also the parametrization

$$\bar{\mathcal{E}}(\rho, x_p) = \bar{\mathcal{E}}\left(\rho, \frac{1}{2}\right) + C_s \left(\frac{\rho}{\rho_0}\right)^\gamma (1 - 2x_p)^2. \quad (5.5)$$

In using this formula we take $\rho_0 = 0.16 \text{ fm}^{-3}$, the standard value for nuclear matter saturation.

By fitting $S(\rho)$, shown in Fig. 8, with Eq. (5.5) within the density range $\rho \in [0.7, 3.1] \times 10^{-2} \text{ fm}^{-3}$, the free parameters C_s and γ are then determined. In the chosen density range $S(\rho)$ has a smooth behavior, once the region around the maximum of $\bar{\mathcal{E}}$ for SNM in Fig. 4 is clearly left behind. The values

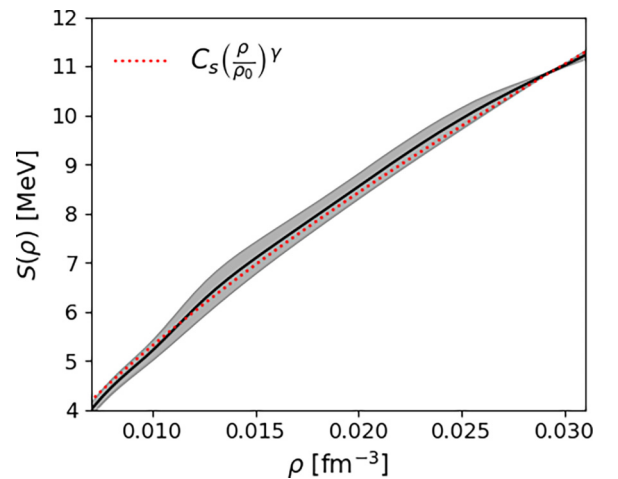


FIG. 8. The solid line and its uncertainty band correspond to the symmetry energy $S(\rho)$ obtained from the resummation of the ladder diagrams as a function of density ρ . The red dashed line is the parametrization of Eq. (5.5) using the fitted central values of C_s and γ in Eq. (5.6).

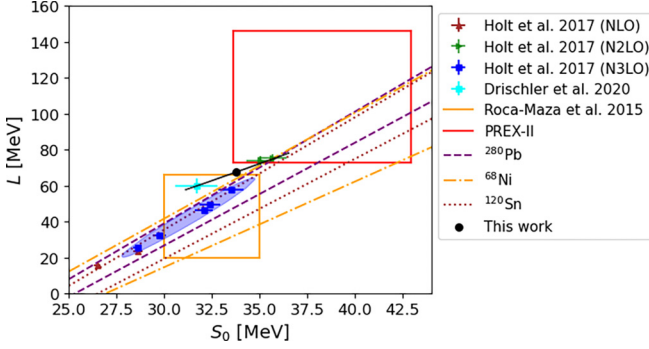


FIG. 9. L vs S_0 at ρ_0 . We show our results their 2σ uncertainty by the black circle and area, respectively. We also give the outcome of Ref. [50] at different orders in the perturbative chiral expansion: NLO (Holt *et al.* [50]), N2LO (Holt *et al.* [50]), and N3LO (Holt *et al.* [50]). The 2σ uncertainty area of the last is shown in blue. Three empirical bands, obtained in Ref. [63] by analyzing the static dipole polarizability in the nuclei ^{208}Pb , ^{68}Ni , and ^{120}Sn , are plotted. The inferred values from the same reference are also reported by the orange square (Roca-Maza *et al.*, 2015 [63]). The result of Ref. [64] is given by the cyan point (Drischler *et al.*, 2020 [64]), and the interval of values from the recent experiment PREX-II [65] corresponds to the red square (PREX-II [65]).

obtained from the fit are

$$\begin{aligned} C_s &= 34.77 \pm 0.15 \text{ MeV}, \\ \gamma &= 0.667 \pm 0.003. \end{aligned} \quad (5.6)$$

By employing the central values and the parametrization of Eq. (5.5) we obtain the red dashed line plotted in Fig. 8, which shows that the fit closely reproduce the results from the ladder resummation for $\rho \in [0.7, 3.1] \times 10^{-2} \text{ fm}^{-3}$.

The parametrization in Eq. (5.5) fixed at low densities allows us to extend the results to larger values of ρ and, in particular, consider the values for the symmetry energy at saturation $S_0 \equiv S(\rho_0)$,

$$S_0 = \bar{\mathcal{E}}(\rho_0, 0) - \bar{\mathcal{E}}(\rho_0, \frac{1}{2}), \quad (5.7)$$

and its slope

$$L = 3\rho_0 \left. \frac{dS(\rho)}{d\rho} \right|_{\rho_0} = 3C_s\gamma_s. \quad (5.8)$$

These are magnitudes of phenomenological interest, with special attention devoted to the investigation of existing correlations between these quantities (defined and computed in infinite nuclear matter) and measured observables. Among the latter we have those in finite nuclei, such as the neutron skin thickness in neutron-rich nuclei and the electric dipole polarizability, and others in astrophysics, e.g., concerning neutron stars and heavy-ion collisions with radioactive beams [28,63,66,67].

We show our central values for S_0 and L in Fig. 9 by the black circle corresponding to $S_0 = 33.77 \text{ MeV}$ and $L = 67.59 \text{ MeV}$. The 2σ uncertainty area is also given by the black narrow area, extending over the values $31.10 \leq S_0 \leq 36.57 \text{ MeV}$ and $57.82 \leq L \leq 78.29 \text{ MeV}$. The figure also gives the phenomenological bands obtained in Ref. [63] by

analyzing the data on the electric dipole polarizabilities of ^{68}Ni , ^{120}Sn , and ^{208}Pb , employing several density functionals. The same reference infers the intervals of values $30 \leq S_0 \leq 35 \text{ MeV}$ and $20 \leq L \leq 66 \text{ MeV}$, represented by the orange square in Fig. 9. We also show the outcome of Ref. [50] obtained by employing chiral perturbation theory at different orders, as indicated in the figure. The 2σ correlation area at N3LO of Ref. [50] is given by the blue area, and lies quite close to our outcome. The result from the recent Bayesian statistical analysis of [64] is shown by the cyan dot, and that from the recent experiment PREX-II [65], $S_0 = 38.29 \pm 4.66 \text{ MeV}$ and $L = 109.56 \pm 36.41 \text{ MeV}$, corresponds to the red square, which is compatible with our extrapolation.

VI. CONCLUSIONS

We have studied infinite nuclear matter by resumming the series of ladder diagrams following the results of Ref. [31]. The master formula there given allows one to consider arbitrary nucleon-nucleon (NN) interactions in vacuum. This formalism can be explicitly solved for the case of NN interactions driven by contact-interaction potentials. The partial-wave amplitudes up to and including G waves are considered for symmetric and pure neutron matter for Fermi momentum up to 150 MeV, so that the results are convergent under the inclusion of higher partial-wave amplitudes. The energy per particle $\bar{\mathcal{E}}$ obtained from the ladder series is renormalized, without any dependence on arbitrary scales, such as cutoffs or regulators, and it is directly expressed in terms of the experimental NN phase shifts and mixing angles, reducing the systematic errors in the calculation of dilute nuclear matter. The knowledge of $\bar{\mathcal{E}}$ as a function of density ρ allows also studying other interesting observables such as the pressure $P(\rho)$ (equation of state) and the sound velocity $c_s(\rho)$.

We notice that our results are specially suitable in the low density region where a pionless description of NN interactions can make sense. They comprise the full vacuum NN interactions and the leading order nonperturbative in-medium contributions, according to the power counting of Ref. [25]. An interesting application of these results given by the resummation of the ladder diagrams would be to use them to constrain the many-body techniques employed in deriving the equations of state for higher densities that are used to calculate neutron star properties. We also plan to extend our present results by taking into account finite-range NN interactions and, in this way, being able to reach higher densities $\rho \gtrsim \rho_0$. Work along these lines is in progress.

ACKNOWLEDGMENTS

We would like to thank interesting discussions with Felipe J. Llanes-Estrada and Eva Lope-Oter. This work has been supported in part by the MICINN AEI (Spain) Grants No. PID2019-106080GB-C21/AEI/10.13039/501100011033 and No. PID2019-106080GB-C22/AEI/10.13039/501100011033, and by the EU Horizon 2020 research and innovation program, STRONG-2020 project, under Grant Agreement No. 824093.

APPENDIX A: TECHNICAL STEPS FOR DERIVING THE IEs FOR $t_m(\mathbf{a}\hat{\mathbf{z}})$

In order to arrive to the IE for $t_m(\mathbf{a})$ in Eq. (3.4), let us first analyze the matrix elements of the kernel $G(p) - L_m(p, \mathbf{a})$ between antisymmetrized plane-wave states. We take the expressions in Eqs. (3.2) and (2.9) for the operators $G(p)$ and $L_m(p, \mathbf{a})$, respectively. From the operator $G(p)$ we then have from Eq. (3.2) that

$${}_A\langle \mathbf{k}'\tilde{\sigma}'_1\tilde{\sigma}'_2\tilde{\alpha}'_1\tilde{\alpha}'_2 | G(p) | \mathbf{k}\tilde{\sigma}_1\tilde{\sigma}_2\tilde{\alpha}_1\tilde{\alpha}_2 \rangle_A = -\frac{m(2\pi)^3}{k^2 - p^2 - i\epsilon} \left[\delta(\mathbf{k}' - \mathbf{k})\delta_{\tilde{\sigma}'_1\tilde{\sigma}_1}\delta_{\tilde{\sigma}'_2\tilde{\sigma}_2}\delta_{\tilde{\alpha}'_1\tilde{\alpha}_1}\delta_{\tilde{\alpha}'_2\tilde{\alpha}_2} - \delta(\mathbf{k}' + \mathbf{k})\delta_{\tilde{\sigma}'_1\tilde{\sigma}_2}\delta_{\tilde{\sigma}'_2\tilde{\sigma}_1}\delta_{\tilde{\alpha}'_1\tilde{\alpha}_2}\delta_{\tilde{\alpha}'_2\tilde{\alpha}_1} \right]. \quad (\text{A1})$$

For the case of the operator $L_m(p, \mathbf{a})$, Eq. (2.9), more care is needed because the dependence of the Fermi momenta on the isospin indices of the intermediate states, $\tilde{\alpha}_1$ and $\tilde{\alpha}_2$. Namely,

$$\begin{aligned} {}_A\langle \mathbf{k}'\tilde{\sigma}'_1\tilde{\sigma}'_2\tilde{\alpha}'_1\tilde{\alpha}'_2 | L_m(p, \mathbf{a}) | \mathbf{k}\tilde{\sigma}_1\tilde{\sigma}_2\tilde{\alpha}_1\tilde{\alpha}_2 \rangle_A &= -\frac{(2\pi)^3 m}{k^2 - p^2 - i\epsilon} \left[\delta(\mathbf{k}' - \mathbf{k})\delta_{\tilde{\sigma}'_1\tilde{\sigma}_1}\delta_{\tilde{\sigma}'_2\tilde{\sigma}_2}\delta_{\tilde{\alpha}'_1\tilde{\alpha}_1}\delta_{\tilde{\alpha}'_2\tilde{\alpha}_2} - \delta(\mathbf{k}' + \mathbf{k})\delta_{\tilde{\sigma}'_1\tilde{\sigma}_2}\delta_{\tilde{\sigma}'_2\tilde{\sigma}_1}\delta_{\tilde{\alpha}'_1\tilde{\alpha}_2}\delta_{\tilde{\alpha}'_2\tilde{\alpha}_1} \right] \\ &\times \left[\theta(\xi_{\tilde{\alpha}_1} - |\mathbf{k} + \mathbf{a}|) + \theta(\xi_{\tilde{\alpha}_2} - |\mathbf{k} - \mathbf{a}|) \right]. \end{aligned} \quad (\text{A2})$$

The sum over the two Heaviside functions factorizes because the sum over the intermediate states is symmetric under the simultaneous exchange of the subscripts $1 \leftrightarrow 2$ and $\mathbf{q} \rightarrow -\mathbf{q}$.

Putting together these results, we end with the following expression for the operator $-V[G(p) - L_m(p, \mathbf{a})]t_m(\mathbf{a})$,

$$\begin{aligned} &-V[G(p) - L_m(p, \mathbf{a})]t_m(\mathbf{a}) \\ &= -\frac{1}{2^2} \sum_{\tilde{\sigma}, \tilde{\sigma}', \tilde{\alpha}, \tilde{\alpha}'} \int \frac{d^3 k'}{(2\pi)^3} \frac{d^3 k}{(2\pi)^3} V | \mathbf{k}'\tilde{\sigma}'_1\tilde{\sigma}'_2\tilde{\alpha}'_1\tilde{\alpha}'_2 \rangle_{AA} \langle \mathbf{k}'\tilde{\sigma}'_1\tilde{\sigma}'_2\tilde{\alpha}'_1\tilde{\alpha}'_2 | G(p) - L_m(p, \mathbf{a}) | \mathbf{k}, \tilde{\sigma}_1\tilde{\sigma}_2\tilde{\alpha}_1\tilde{\alpha}_2 \rangle_{AA} \langle \mathbf{k}\tilde{\sigma}_1\tilde{\sigma}_2\tilde{\alpha}_1\tilde{\alpha}_2 | t_m(\mathbf{a}) \\ &= \frac{m}{2} \sum_{\tilde{\sigma}, \tilde{\alpha}} \int \frac{d^3 k}{(2\pi)^3} V | \mathbf{k}\tilde{\sigma}_1\tilde{\sigma}_2\tilde{\alpha}_1\tilde{\alpha}_2 \rangle_A \frac{1 - \theta(\xi_{\tilde{\alpha}_1} - |\mathbf{k} + \mathbf{a}|) - \theta(\xi_{\tilde{\alpha}_2} - |\mathbf{k} - \mathbf{a}|)}{k^2 - p^2 - i\epsilon} {}_A\langle \mathbf{k}\tilde{\sigma}_1\tilde{\sigma}_2\tilde{\alpha}_1\tilde{\alpha}_2 | t_m(\mathbf{a}). \end{aligned} \quad (\text{A3})$$

Then, taking the previous result in Eq. (3.3), the IE Eq. (3.4) for the two-body scattering operator in momentum space follows.

From the decomposition of the antisymmetrized plane-wave states in the partial-wave basis, Eq. (2.17), Eq. (A3) for $-V[G(p) - L_m(p, \mathbf{a})]t_m(\mathbf{a})$ in the partial-wave basis is

$$\begin{aligned} &-V[G(p) - L_m(p, \mathbf{a})]t_m(\mathbf{a}) \\ &= m \sum_{\tilde{\sigma}, \tilde{\alpha}} \sum_{J\mu\ell m_3} \sum_{S_3 I_3} \sum_{J'\mu'\ell' S'I'_3 k} \int \frac{d^3 k}{(2\pi)^2} V | J'\mu'\ell' S'I'_3 k \rangle \frac{1 - \theta(\xi_{\tilde{\alpha}_1} - |\mathbf{k} + \mathbf{a}|) - \theta(\xi_{\tilde{\alpha}_2} - |\mathbf{k} - \mathbf{a}|)}{k^2 - p^2 - i\epsilon} \langle J\mu\ell S I_3 k | t_m(\mathbf{a}) \rangle \chi(S\ell I) \chi(S'\ell'I') \\ &\times (\tilde{\sigma}_1\tilde{\sigma}_2 s'_3 | s s S') (\tilde{\sigma}_1\tilde{\sigma}_2 s_3 | s s S) (\tilde{\alpha}_1\tilde{\alpha}_2 i'_3 | \tau \tau I') (\tilde{\alpha}_1\tilde{\alpha}_2 i_3 | \tau \tau I) (m'_3 s'_3 \mu' | \ell' S' J') (m_3 s_3 \mu | \ell S J) Y_{\ell'}^{m'_3}(\hat{\mathbf{k}})^* Y_{\ell}^{m_3}(\hat{\mathbf{k}}), \end{aligned} \quad (\text{A4})$$

where $s = \tau = 1/2$ is the spin and isospin of the each nucleon, respectively. It is also clear from this equation that $i_3 = i'_3 = \tilde{\alpha}_1 + \tilde{\alpha}_2$. The sum over $\tilde{\sigma}_1$ and $\tilde{\sigma}_2$ can be readily done because of the orthogonality properties of the Clebsch-Gordan coefficients:

$$\sum_{\tilde{\sigma}_1, \tilde{\sigma}_2} (\tilde{\sigma}_1\tilde{\sigma}_2 s'_3 | s s S') (\tilde{\sigma}_1\tilde{\sigma}_2 s_3 | s s S) = \delta_{s'_3 s_3} \delta_{S' S}. \quad (\text{A5})$$

In the following we choose \mathbf{a} along the z axis because this is enough to calculate $\mathcal{E}_{\mathcal{L}}$ [cf. Eq. (2.18)], and it also induces extra simplifications in the final IE for $t_m(\mathbf{a}\hat{\mathbf{z}})$. Because of this choice it is clear that there is no dependence on the azimuthal angle of \mathbf{k} in the integral of Eq. (A3), because $|\mathbf{k} \pm \mathbf{a}\hat{\mathbf{z}}|$ only depends on its polar angle. Thus,

$$\int_0^{2\pi} d\varphi Y_{\ell'}^{m'_3}(\theta, \varphi)^* Y_{\ell}^{m_3}(\theta, \varphi) \propto \delta_{m'_3 m_3}. \quad (\text{A6})$$

As a result $\mu' = \mu$ because $\mu' = s'_3 + m'_3 = s_3 + m_3 = \mu$. Then, we can get rid of the sums over $\tilde{\sigma}_1$, $\tilde{\sigma}_2$, S' , s'_3 , m'_3 , μ' , and i'_3 in Eq. (A4), which then becomes

$$\begin{aligned} &-V[G(p) - L_m(p, \mathbf{a})]t_m(\mathbf{a}\hat{\mathbf{z}}) \\ &= m \sum_{\tilde{\alpha}_1, \tilde{\alpha}_2} \sum_{J\mu\ell m_3} \sum_{S_3 I_3} \sum_{J'\mu\ell' S'I_3 k} \int \frac{d^3 k}{(2\pi)^2} V | J'\mu\ell' S'I_3 k \rangle \frac{1 - \theta(\xi_{\tilde{\alpha}_1} - |\mathbf{k} + \mathbf{a}\hat{\mathbf{z}}|) - \theta(\xi_{\tilde{\alpha}_2} - |\mathbf{k} - \mathbf{a}\hat{\mathbf{z}}|)}{k^2 - p^2 - i\epsilon} \langle J\mu\ell S I_3 k | t_m(\mathbf{a}\hat{\mathbf{z}}) \rangle \chi(S\ell I) \chi(S'\ell'I') \\ &\times (\tilde{\alpha}_1\tilde{\alpha}_2 i_3 | \tau \tau I') (\tilde{\alpha}_1\tilde{\alpha}_2 i_3 | \tau \tau I) (m_3 s_3 \mu | \ell' S' J') (m_3 s_3 \mu | \ell S J) Y_{\ell'}^{m_3}(\hat{\mathbf{k}})^* Y_{\ell}^{m_3}(\hat{\mathbf{k}}). \end{aligned} \quad (\text{A7})$$

We then continue with the case $i_3 = 0$ and deduce the corresponding IE for the $t_m(a\hat{\mathbf{z}})$, and take first Eq. (A7) with $I' \neq I$, $i_3 = 0$. For $\tau = 1/2$ we then have the following substructure within the integrand:

$$\begin{aligned} & \frac{1 - (-1)^{I'-I}}{2} \sum_{\tilde{\alpha}_1, \tilde{\alpha}_2} (\tilde{\alpha}_1 \tilde{\alpha}_2 i_3 | \tau \tau I') (\tilde{\alpha}_1 \tilde{\alpha}_2 i_3 | \tau \tau I) [1 - \theta(\xi_{\tilde{\alpha}_1} - |\mathbf{k} + a\hat{\mathbf{z}}|) - \theta(\xi_{\tilde{\alpha}_2} - |\mathbf{k} - a\hat{\mathbf{z}}|)] \\ &= \frac{1 - (-1)^{I'-I}}{4} [-\theta(\xi_1 - |\mathbf{k} + a\hat{\mathbf{z}}|) - \theta(\xi_2 - |\mathbf{k} - a\hat{\mathbf{z}}|) + \theta(\xi_2 - |\mathbf{k} + a\hat{\mathbf{z}}|) + \theta(\xi_1 - |\mathbf{k} - a\hat{\mathbf{z}}|)], \end{aligned} \quad (\text{A8})$$

where in order to simplify the notation the Fermi momenta $\xi_{\tilde{\alpha}_i}$ are denoted as

$$\begin{aligned} \xi_1 &\equiv \xi_{+\frac{1}{2}}, \\ \xi_2 &\equiv \xi_{-\frac{1}{2}}. \end{aligned} \quad (\text{A9})$$

Next, we notice that $(-1)^{\ell'} = -(-1)^\ell$ because $I' \neq I$, the total spin S is the same and there is contribution only when the Fermi statistics factors $\chi(S\ell I)$, $\chi(S\ell' I') \neq 0$. Then, by exchanging $\mathbf{k} \rightarrow -\mathbf{k}$ in the last two step functions in Eq. (A8), taking into account the parity rule for the spherical harmonics, $Y_\ell^m(-\mathbf{k}) = (-1)^\ell Y_\ell^m(\mathbf{k})$, the contributions in Eq. (A7) with $I' \neq I$ become

$$\begin{aligned} & -m \sum_{\substack{J\mu\ell m_3 \\ S_3 I_3}} \sum_{J'\ell'I'} \frac{1 - (-1)^{I'-I}}{2} \int \frac{d^3k}{(2\pi)^2} \frac{V |J'\mu\ell' S'I' i_3 k\rangle \langle J\mu\ell S I i_3 k | t_m(a\hat{\mathbf{z}})}{k^2 - p^2 - i\epsilon} Y_{\ell'}^{m_3}(\hat{\mathbf{k}}) Y_\ell^{m_3}(\hat{\mathbf{k}}) \chi(S\ell I) \chi(S\ell' I') \\ & \times (m_3 s_3 \mu | \ell' S J') (m_3 s_3 \mu | \ell S J) [\theta(\xi_1 - |\mathbf{k} + a\hat{\mathbf{z}}|) + \theta(\xi_2 - |\mathbf{k} - a\hat{\mathbf{z}}|)]. \end{aligned} \quad (\text{A10})$$

On the other hand, for those with $I' = I$ we have that $(\tilde{\alpha}_1 \tilde{\alpha}_2 i_3 | \tau \tau I)^2 = 1/2$ in all cases, and the sum over the isospin indices $\tilde{\alpha}_1$ and $\tilde{\alpha}_2$ gives

$$\frac{1 + (-1)^{I'-I}}{4} \chi(S\ell I) \chi(S\ell' I') [2 - \theta(\xi_1 - |\mathbf{k} + a\hat{\mathbf{z}}|) - \theta(\xi_2 - |\mathbf{k} - a\hat{\mathbf{z}}|) - \theta(\xi_2 - |\mathbf{k} + a\hat{\mathbf{z}}|) - \theta(\xi_1 - |\mathbf{k} - a\hat{\mathbf{z}}|)] Y_{\ell'}^{m_3}(\mathbf{k}) Y_\ell^{m_3}(\mathbf{k}). \quad (\text{A11})$$

Since now $(-1)^\ell = (-1)^{\ell'}$ because S is conserved, $I' = I$, and there is contribution only for $\chi(S\ell I)$, $\chi(S\ell' I') \neq 0$, the exchange $\mathbf{k} \rightarrow -\mathbf{k}$ implies that the contributions in Eq. (A7) with $I' = I$ read

$$\begin{aligned} & m \sum_{\substack{J\mu\ell m_3 \\ S_3 I_3}} \sum_{J'\ell'I'} \frac{1 + (-1)^{I'-I}}{2} \int \frac{d^3k}{(2\pi)^2} \chi(S\ell I) \chi(S\ell' I') (m_3 s_3 \mu | \ell' S J') (m_3 s_3 \mu | \ell S J) Y_{\ell'}^{m_3}(\hat{\mathbf{k}}) Y_\ell^{m_3}(\hat{\mathbf{k}}) \\ & \times V |J'\mu\ell' S'I' i_3 k\rangle \frac{1 - \theta(\xi_1 - |\mathbf{k} + a\hat{\mathbf{z}}|) - \theta(\xi_2 - |\mathbf{k} - a\hat{\mathbf{z}}|)}{k^2 - p^2 - i\epsilon} \langle J\mu\ell S I i_3 k | t_m(a\hat{\mathbf{z}}). \end{aligned} \quad (\text{A12})$$

Putting together Eqs. (A10) and (A12), the resulting IE reads

$$\begin{aligned} \langle J'\mu\ell' S'I' i_3 p' | t_m(a\hat{\mathbf{z}}) | J\mu\ell S I i_3 p \rangle &= \langle J'\mu\ell' S'I' i_3 p' | V | J\mu\ell S I i_3 p \rangle + m \sum_{\substack{J_1 \ell_1 m_3 \\ S_3 \ell_2 I_1}} \int \frac{d^3k}{(2\pi)^2} \frac{\chi(S\ell_2 I') \chi(S\ell_1 I_1)}{k^2 - p^2 - i\epsilon} (m_3 s_3 \mu | \ell_2 S J') \\ & \times (m_3 s_3 \mu | \ell_1 S J_1) Y_{\ell_2}^{m_3}(\hat{\mathbf{k}}) Y_{\ell_1}^{m_3}(\hat{\mathbf{k}}) \langle J'\mu\ell' S'I' i_3 p' | V | J'\mu\ell_2 S'I' i_3 k \rangle \langle J_1 \mu \ell_1 S I_1 i_3 k | t_m(a\hat{\mathbf{z}}) | J\mu\ell S I i_3 p \rangle \\ & \times \left\{ \frac{1 + (-1)^{I'-I_1}}{2} - \theta(\xi_1 - |\mathbf{k} + a\hat{\mathbf{z}}|) - \theta(\xi_2 - |\mathbf{k} - a\hat{\mathbf{z}}|) \right\}, \end{aligned} \quad (\text{A13})$$

where we have taken into account that the potential V conserves isospin. Now, since the combination $1 + (-1)^{I'-I_1}$ conserves isospin, this implies that

$$\int d\mathbf{k} Y_{\ell_2}^{m_3}(\hat{\mathbf{k}}) Y_{\ell_1}^{m_3}(\hat{\mathbf{k}}) \chi(S\ell_2 I') \chi(S\ell_1 I_1) \frac{1 + (-1)^{I'-I_1}}{2} = \int d\mathbf{k} Y_{\ell_2}^{m_3}(\hat{\mathbf{k}}) Y_{\ell_1}^{m_3}(\hat{\mathbf{k}}) \chi(S\ell_2 I') \chi(S\ell_1 I_1), \quad (\text{A14})$$

by simply exchanging $\hat{\mathbf{k}} \rightarrow -\hat{\mathbf{k}}$ in the original integral, and taking into account that Fermi statistics requires then that $(-1)^{\ell_2} = (-1)^{\ell_1}$ for $I' = I_1$, and $(-1)^{\ell_2} = -(-1)^{\ell_1}$ for $I' \neq I_1$. Taking this result into Eq. (A13), one ends with the simpler expression of Eq. (3.5).

APPENDIX B: SOME SYMMETRY PROPERTIES OF PWAs: GENERAL VALUES FOR ξ_1, ξ_2

Let us show that we do not really need to calculate the PWAs of $t_m(a\hat{\mathbf{z}})$ with negative μ since they obey the rule

$$\langle J' - \mu\ell' SI_3 p' | t_m(a\hat{\mathbf{z}}) | J - \mu\ell SI_3 p \rangle = (-1)^{\ell'+\ell+J'+J} \langle J' \mu\ell' SI' i_3 p' | t_m(a\hat{\mathbf{z}}) | J \mu\ell SI_3 p \rangle. \quad (\text{B1})$$

To prove it we start by considering the IE of Eq. (3.5) for the PWAs with $-\mu$. Because of rotational symmetry the matrix elements of V are independent of μ . We also employ the symmetry property of the Clebsch-Gordan coefficients under the change of sign of the third components of spin [68]; then

$$(m_3\sigma_3 - \mu|\ell_2 SJ')(m_3\sigma_3 - \mu|\ell_1 SJ_1) = (-1)^{\ell_2+\ell_1+J'+J_1} (-m_3 - \sigma_3\mu|\ell_2 SJ')(-m_3 - \sigma_3\mu|\ell_1 SJ_1). \quad (\text{B2})$$

Next, we take into account that the product of the two spherical harmonics is real and we can write

$$Y_{\ell_2}^{m_3}(\hat{\mathbf{k}}) Y_{\ell_1}^{m_3}(\mathbf{k}) = Y_{\ell_2}^{m_3}(\hat{\mathbf{k}}) Y_{\ell_1}^{m_3}(\mathbf{k})^* = Y_{\ell_2}^{-m_3}(\hat{\mathbf{k}}) Y_{\ell_1}^{-m_3}(\mathbf{k}), \quad (\text{B3})$$

where we have also exchanged the sign of the third components of the angular momenta by making use of the well-known property $Y_\ell^m(\hat{\mathbf{k}})^* = (-1)^m Y_\ell^{-m}(\hat{\mathbf{k}})$.

Implementing this procedure, the IE for $(-1)^{\ell'+\ell+J'+J} \langle J' - \mu\ell' SI_3 p' | t_m(a\hat{\mathbf{z}}) | J - \mu\ell SI_3 p \rangle$ from Eq. (3.5) becomes

$$\begin{aligned} & (-1)^{\ell'+\ell+J'+J} \langle J' - \mu\ell' SI' i_3 p' | t_m(a\hat{\mathbf{z}}) | J - \mu\ell SI_3 p \rangle \\ &= \underbrace{(-1)^{\ell'+\ell+J'+J}}_{+1} \underbrace{\langle J' \mu\ell' SI' i_3 p' | V | J \mu\ell SI_3 p \rangle}_{\propto \delta_{J'J} \delta_{\ell'\ell} \delta_{\ell+\text{mod}(2)}} + m \sum_{\substack{J_1 \ell_1 m_3 \\ s_3 \ell_2 I_1}} \int \frac{d^3k}{(2\pi)^2} \frac{\chi(S\ell_2 I') \chi(S\ell_1 I_1)}{k^2 - p^2 - i\epsilon} \\ &\quad \times (-m_3 - s_3\mu|\ell_2 SJ') (-m_3 - s_3\mu|\ell_1 SJ_1) Y_{\ell_2}^{-m_3}(\hat{\mathbf{k}}) Y_{\ell_1}^{-m_3}(\mathbf{k}) \underbrace{(-1)^{J'+\ell'+J'+\ell_2}}_{+1} \underbrace{\langle J' \mu\ell' SI' i_3 p' | V | J' \mu\ell_2 SI' i_3 k \rangle}_{\propto \delta_{\ell'\ell_2} \delta_{\ell_2+\text{mod}(2)}} \\ &\quad \times (-1)^{J_1+\ell_1+J+\ell} \langle J_1 \mu\ell_1 SI_1 i_3 k | t_m(a\hat{\mathbf{z}}) | J \mu\ell SI_3 p \rangle [1 - \theta(\xi_1 - |\mathbf{k} + a\hat{\mathbf{z}}|) - \theta(\xi_2 - |\mathbf{k} - a\hat{\mathbf{z}}|)]. \end{aligned} \quad (\text{B4})$$

This IE, after relabeling the dummy indices $-m_3 \rightarrow m_3$ and $-s_3 \rightarrow s_3$ (which also has a symmetric sum interval around zero), is actually the same IE as the one satisfied by $\langle J' \mu\ell' SI' i_3 p' | t_m(a\hat{\mathbf{z}}) | J \mu\ell SI_3 p \rangle$, and Eq. (B1) follows.

As a corollary of Eq. (B1) we notice that for $\mu_1 = 0$ it is necessary that

$$(-1)^{J'+J} = (-1)^{\ell'+\ell}, \quad (\text{B5})$$

otherwise the PWA is zero.

The PWAs of $t_m(a\hat{\mathbf{z}})$ are symmetric under the exchange of the initial and final quantum numbers, namely,

$$\langle J' \mu\ell' SI' i_3 p' | t_m(a\hat{\mathbf{z}}) | J \mu\ell SI_3 p \rangle = \langle J \mu\ell SI_3 p' | t_m(a\hat{\mathbf{z}}) | J' \mu\ell' SI' i_3 p \rangle \quad (\text{B6})$$

with the scattering energy fixed by p , so that $E = p^2/m$. This relation is particularly useful for the on-shell case with $p' = p$, which is the one needed in the evaluation of $\mathcal{E}_{\mathcal{H}}$. It implies then that the in-medium on-shell T matrix is symmetric under the exchange of the discrete labels.

For the demonstration we use that the matrix elements of V because of time reversal are invariant under the exchange of the initial and final states between them. Therefore, the IE for $\langle J \mu\ell SI_3 p | t_m(a\hat{\mathbf{z}}) | J' \mu\ell' SI' i_3 p' \rangle$ from Eq. (3.5) reads

$$\begin{aligned} \langle J \mu\ell SI_3 p | t_m(a\hat{\mathbf{z}}) | J' \mu\ell' SI' i_3 p' \rangle &= \langle J' \mu\ell' SI' i_3 p' | V | J \mu\ell SI_3 p \rangle + m \sum_{\substack{J_1 \ell_1 m_3 \\ s_3 \ell_2 I_1}} \int \frac{d^3k}{(2\pi)^2} \frac{\chi(S\ell_2 I') \chi(S\ell_1 I_1)}{k^2 - p^2 - i\epsilon} (m_3 s_3 \mu | \ell_2 SJ) (m_3 s_3 \mu | \ell_1 SJ_1) \\ &\quad \times \underbrace{Y_{\ell_2}^{m_3}(\hat{\mathbf{k}}) Y_{\ell_1}^{m_3}(\mathbf{k})^*}_{\text{It is real. The complex conjugate is taken}} \langle J_1 \mu\ell_1 SI_1 i_3 k | t_m(a\hat{\mathbf{z}}) | J' \mu\ell' SI' i_3 p' \rangle \\ &\quad \times \langle J \mu\ell_2 SI_3 k | V | J \mu\ell SI_3 p \rangle [1 - \theta(\xi_1 - |\mathbf{k} + a\hat{\mathbf{z}}|) - \theta(\xi_2 - |\mathbf{k} - a\hat{\mathbf{z}}|)]. \end{aligned} \quad (\text{B7})$$

This is the same IE as the one satisfied by $\langle J' \mu\ell' SI' i_3 p' | t_m(a\hat{\mathbf{z}}) | J \mu\ell SI_3 p \rangle$ as we wanted to show. In order to arrive to this conclusion we have used the fact that the operational equation for $t_m(\mathbf{a})$ of Eq. (3.3) can also be rewritten as

$$t_m(\mathbf{a}) = V - t_m(\mathbf{a})[G - L_m(p, \mathbf{a})]V. \quad (\text{B8})$$

- [1] A. Fetter and J. Walecka, *Quantum Theory of Many-Particle Systems* (McGraw-Hill, New York, 1971).
- [2] K. Huang and C. Yang, *Phys. Rev.* **105**, 767 (1957).
- [3] T. Lee and C. Yang, *Phys. Rev.* **105**, 1119 (1957).
- [4] V. N. Efimov and M. Y. Amusia, *Sov. Phys. JETP* **20**, 388 (1965).
- [5] M. Y. Amusia and V. N. Efimov, *Ann. Phys. (NY)* **47**, 377 (1968).
- [6] G. A. Baker, *Rev. Mod. Phys.* **43**, 479 (1971).
- [7] B. F. Bishop, *Ann. Phys. (NY)* **77**, 106 (1973).
- [8] H. Hammer and R. Furnstahl, *Nucl. Phys. A* **678**, 277 (2000).
- [9] E. W. Zwerger, *The BCS-BEC Crossover and the Unitary Fermi Gas*, Lecture Notes in Physics (Springer-Verlag, Berlin, 2012), Vol. 836.
- [10] S. Giorgini, L. P. Pitaevskii, and S. Stringari, *Rev. Mod. Phys.* **80**, 1215 (2008).
- [11] M. Randeria and E. Taylor, *Annu. Rev. Condens. Matter Phys.* **5**, 209 (2014).
- [12] Q. Chen *et al.*, *Phys. Rev. C* **77**, 054002 (2008).
- [13] H. Bethe, *Physica* **22**, 987 (1956).
- [14] K. Brueckner, C. Levinson, and H. Mahmoud, *Phys. Rev.* **95**, 217 (1954).
- [15] K. Brueckner, *Phys. Rev.* **96**, 508 (1954).
- [16] K. Brueckner, *Phys. Rev.* **97**, 1353 (1955).
- [17] J. Hu, Y. Zhang, E. Epelbaum, Ulf-G. Meißner, and J. Meng, *Phys. Rev. C* **96**, 034307 (2017).
- [18] D. Thouless, *Ann. Phys.* **10**, 553 (1960).
- [19] J. V. Steele, *arXiv:nucl-th/0010066*.
- [20] A. Lacour, J. A. Oller, and U.-G. Meißner, *Ann. Phys. (NY)* **326**, 241 (2011).
- [21] N. Kaiser, *Nucl. Phys. A* **860**, 41 (2011).
- [22] N. Kaiser, *Eur. Phys. J. A* **48**, 148 (2012).
- [23] T. Schäfer, C.-W. Kao, and S. R. Cotanch, *Nucl. Phys. A* **762**, 82 (2005).
- [24] C. Drischler, K. Hebeler, and A. Schwenk, *Phys. Rev. Lett.* **122**, 042501 (2019).
- [25] J. A. Oller, A. Lacour, and U. G. Meißner, *J. Phys. G: Nucl. Part. Phys.* **37**, 015106 (2010).
- [26] U.-G. Meißner, J. A. Oller, and A. Wirzba, *Ann. Phys. (NY)* **297**, 27 (2002).
- [27] A. Boulet and D. Lacroix, *J. Phys. G: Nucl. Part. Phys.* **46**, 105104 (2019).
- [28] M. Grasso, *Prog. Part. Nucl. Phys.* **106**, 256 (2019).
- [29] U. van Kolck, *Few-Body Syst.* **58**, 112 (2017).
- [30] S. König, H. W. Griesshammer, H.-W. Hammer, and U. van Kolck, *Phys. Rev. Lett.* **118**, 202501 (2017).
- [31] J. M. Alarcón and J. A. Oller, *Ann. Phys. (NY)* **437**, 168741 (2022).
- [32] J. A. Oller, *Phys. Rev. C* **65**, 025204 (2002).
- [33] S. Goda and D. Jido, *Phys. Rev. C* **88**, 065204 (2013).
- [34] S. Goda and D. Jido, *Prog. Theor. Exp. Phys.* **2014**, 033D03 (2014).
- [35] A. Lacour, J. A. Oller, and U.-G. Meißner, *J. Phys. G: Nucl. Part. Phys.* **37**, 125002 (2010).
- [36] A. Dobado, F. J. Llanes-Estrada, and J. A. Oller, *Phys. Rev. C* **85**, 012801(R) (2012).
- [37] J. A. Oller, *J. Phys. G: Nucl. Part. Phys.* **46**, 073001 (2019).
- [38] J. M. Alarcón and J. A. Oller, *Phys. Rev. C* **106**, 054003 (2022).
- [39] J. A. Oller and D. Entem, *Ann. Phys. (NY)* **411**, 167965 (2019).
- [40] J. A. Oller and E. Oset, *Phys. Rev. D* **60**, 074023 (1999).
- [41] L. Castillejo, R. Dalitz, and F. Dyson, *Phys. Rev.* **101**, 453 (1956).
- [42] J. Bjorken, *Phys. Rev. Lett.* **4**, 473 (1960).
- [43] R. N. Pérez, J. E. Amaro, and E. Ruiz Arriola, *J. Phys. G: Nucl. Part. Phys.* **43**, 114001 (2016).
- [44] D. R. Entem and J. A. Oller, *Phys. Lett. B* **773**, 498 (2017).
- [45] Z.-H. Guo, J. A. Oller, and G. Ríos, *Phys. Rev. C* **89**, 014002 (2014).
- [46] J. A. Oller, *Phys. Rev. C* **93**, 024002 (2016).
- [47] S. König and H. W. Hammer, *Phys. Rev. C* **83**, 064001 (2011).
- [48] D. Lee and T. Schäfer, *Phys. Rev. C* **72**, 024006 (2005).
- [49] M. Schäfer and B. Bazak, *arXiv:2208.10960*.
- [50] J. W. Holt and N. Kaiser, *Phys. Rev. C* **95**, 034326 (2017).
- [51] S. Huth, C. Wellenhofer, and A. Schwenk, *Phys. Rev. C* **103**, 025803 (2021).
- [52] B. Friedman and V. R. Pandharipande, *Nucl. Phys. A* **361**, 502 (1981).
- [53] A. Bulgac, M. M. Forbes, S. Jin, R. Navarro Perez, and N. Schunck, *Phys. Rev. C* **97**, 044313 (2018).
- [54] H. Shen, H. Toki, K. Oyamatsu, and K. Sumiyoshi, *Nucl. Phys. A* **637**, 435 (1998).
- [55] H. Shen, H. Toki, K. Oyamatsu, and K. Sumiyoshi, *Prog. Theor. Phys.* **100**, 1013 (1998).
- [56] C. J. Horowitz and A. Schwenk, *Nucl. Phys. A* **776**, 55 (2006).
- [57] G. Q. Li, R. Machleidt, and R. Brockmann, *Phys. Rev. C* **45**, 2782 (1992).
- [58] E. Epelbaum, H. Krebs, D. Lee, and U.-G. Meißner, *Eur. Phys. J. A* **40**, 199 (2009).
- [59] G. Wlazłowski, J. W. Holt, S. Moroz, A. Bulgac, and K. J. Roche, *Phys. Rev. Lett.* **113**, 182503 (2014).
- [60] A. Gezerlis and J. Carlson, *Phys. Rev. C* **77**, 032801(R) (2008).
- [61] A. Gezerlis, I. Tews, E. Epelbaum, S. Gandolfi, K. Hebeler, A. Nogga, and A. Schwenk, *Phys. Rev. Lett.* **111**, 032501 (2013).
- [62] S. Gandolfi *et al.*, *Mon. Not. R. Astron. Soc.* **404**, L35 (2010).
- [63] X. Roca-Maza, X. Vinas, M. Centelles, B.K. Agrawal, G. Colo, N. Paar, J. Piekarewicz, and D. Vretenar, *Phys. Rev. C* **92**, 064304 (2015).
- [64] C. Drischler, R. J. Furnstahl, J. A. Melendez, and D. R. Phillips, *Phys. Rev. Lett.* **125**, 202702 (2020).
- [65] B. T. Reed, F. J. Fattoyev, C. J. Horowitz, and J. Piekarewicz, *Phys. Rev. Lett.* **126**, 172503 (2021).
- [66] S. Ghosh, B. K. Pradhan, D. Chatterjee, and J. Schaffner-Bielich, *Front. Astron. Space Sci.* **9**, 864294 (2022).
- [67] M. Oertel, M. Hempel, T. Klähn, and S. Typel, *Rev. Mod. Phys.* **89**, 015007 (2017).
- [68] M. Rose, *Elementary Theory of Angular Momentum* (Dover, Mineola, NY, 1995).